EXAMINATION OF LASER-PRODUCED PRESSURE PULSES IN A GALLIUM ARSENIDE SOLAR CELL

John Frank Jacobson

NAVAL POSTGRADUATE SCHOOL
Monterey, California

THESIS

EXAMINATION OF LASER-PRODUCED PRESSURE PULSES IN A GALLIUM ARSENIDE SOLAR CELL

by

John Frank Jacobson

June 1976

Thesis Advisor: A. W. Cooper

UNCLASSIFIED

SECURITY CLASSIFICATION OF THIS PAGE (When Data Entered)

REPORT DOCUMENTATION PAGE		READ INSTRUCTIONS BEFORE COMPLETING FORM
1. REPORT NUMBER	2. GOVT ACCESSION NO.	3. RECIPIENT'S CATALOG NUMBER
4. TITLE (and Subtitle) Examination of Laser-Produced Pressure Pulses in a Gallium Arsenide Solar Cell		5. TYPE OF REPORT & PERIOD COVERED Master's Thesis; June 1976 6. PERFORMING ORG. REPORT NUMBER
7. AUTHOR(s) John Frank Jacobson		8. CONTRACT OR GRANT NUMBER(s)
9. PERFORMING ORGANIZATION NAME AND ADDRESS Naval Postgraduate School Monterey, California 93940		10. PROGRAM ELEMENT, PROJECT, TASK AREA & WORK UNIT NUMBERS
11. CONTROLLING OFFICE NAME AND ADDRESS Naval Postgraduate School Monterey, California 93940		12. REPORT DATE June 1976 13. NUMBER OF PAGES 126
14. MONITORING AGENCY NAME & ADDRESS(if different from Controlling Office) Naval Postgraduate School Monterey, California 93940		15. SECURITY CLASS. (of this report) Unclassified 15a. DECLASSIFICATION/DOWNGRADING SCHEDULE

16. DISTRIBUTION STATEMENT (of this Report)

Approved for public release; distribution unlimited.

17. DISTRIBUTION STATEMENT (of the abstract entered in Block 20, if different from Report)

18. SUPPLEMENTARY NOTES

19. KEY WORDS (Continue on reverse side if necessary and identify by block number)

Pressure Pulses
GaAs Solar Cells
CO_2 Laser Irradiation
Sandia Quartz Gauge

20. ABSTRACT (Continue on reverse side if necessary and identify by block number)

Pressure pulses caused by irradiation of a model gallium arsenide solar cell with a Carbon Dioxide TEA Laser were examined using power densities of the order of 10^7 watts/cm^2. The pressure pulses were monitored with a Sandia type quartz pressure gauge. It was discovered that the relatively low power densities used were capable of removing the silicon dioxide antireflective and gold contact layers of the solar

DD FORM 1 JAN 73 1473 EDITION OF 1 NOV 65 IS OBSOLETE
S/N 0102-014-6601 |
(Page 1)

UNCLASSIFIED

SECURITY CLASSIFICATION OF THIS PAGE (When Data Entered)

cell after only a few shots of the laser. An exponential relationship between the initial thicknesses of these layers and the pressure pulse generated in the gallium arsenide substrate was indicated for gold contact layers of less than 5000 A thickness. Evidence was found that the principal pressure generation mechanism is thermo-mechanical. Gold films of thickness greater than 5000 A were found to be able to absorb the power densities used with no apparent damage.

Examination of Laser-Produced Pressure Pulses in a Gallium Arsenide Solar Cell

by

John Frank Jacobson
Lieutenant, United States Navy
B.A., University of Nebraska, 1970

Submitted in partial fulfillment of the
requirements for the degree of

MASTER OF SCIENCE IN PHYSICS

from the

NAVAL POSTGRADUATE SCHOOL
June 1976

ABSTRACT

Pressure pulses caused by irradiation of a model gallium arsenide solar cell with a Carbon Dioxide TEA Laser were examined using power densities of the order of 10^7 watts/cm^2. The pressure pulses were monitored with a Sandia type quartz pressure gauge. It was discovered that the relatively low power densities used were capable of removing the silicon dioxide antireflective and gold contact layers of the solar cell after only a few shots of the laser. An exponential relationship between the initial thicknesses of these layers and the pressure pulse generated in the gallium arsenide substrate was indicated for gold contact layers of less than 5000 A thickness. Evidence was found that the principal pressure generation mechanism is thermomechanical. Gold films of thickness greater than 5000 A were found to be able to absorb the power densities used with no apparent damage.

TABLE OF CONTENTS

LIST OF FIGURES

I. INTRODUCTION

The development of solar cells as versatile and dependable sources of power for satellites is well-known. Virtually every long-range space probe launched by the United States or the Soviet Union in the last decade has been powered by photovoltaic devices. Solar cells provided the power that operated the television cameras of the Ranger, Surveyor and Lunar Orbiter spacecraft that made possible detailed photographic studies of the surface of the moon. These devices provided the power for the Mariner probes of the planet Venus. The recent Skylab vehicles also utilized solar cells in their electrical generation systems. The application of solar cell technology has led to the development of the systems of communications, navigational and meteorological satellites currently being employed by the United States and other countries [Ref. 1].

The general construction and characteristics of solar cells are treated in detail by several authors. A good review of these topics is contained in Direct Energy Conversion by S. W. Angrist [Ref. 2]. Of particular note in this treatment is the requirement that for maximum theoretical conversion efficiency the solar cell material should have an energy gap of between 1.1 and 2.3 electron volts. Gallium Arsenide (GaAs) with an energy gap of 1.35 ev. satisfies this condition.

A significant amount of research has been undertaken previously to ascertain the effects of laser irradiation on solar cells and phototransistors. A study of irradiation of phosphorus-doped silicon solar cells by a pulsed laser performed by Giuliani [Ref. 3] identified two permanent damage effects: Below laser energy densities of 5 joules/cm^2 no permanent damage to the phototransistor was observed. Irradiation at these low energy densities was found to increase the photoconductive response of the device, however. At energy densities above 10 joules/cm^2 permanent changes in the electrical characteristics in the form of increased dark current were observed. Examination of phototransistors damaged by laser energy densities in this range enabled Marquardt, Giuliani and Fraser [Ref. 4] to explain this increased dark current. Evidence was found that the melting point of the silicon had been exceeded. A model for phosphorus ion migration was developed by treating the phosphorus as a dilute impurity in a melted silicon matrix and then analyzing the migration of the phosphorus ions as a diffusion problem. The subsequent refreezing of the silicon then traps the ions in their new distribution and causes the increased dark current observed.

As evidenced by the above work a mechanism explaining the changes in the electrical properties of phototransistors under laser irradiation has been developed. However, the mechanical damage done to solar cells by laser radiation has not been so thoroughly examined. By investigation of

the momentum delivered to a GaAs solar cell by laser irradiation it was the intent of the current investigation to amplify the knowledge in this area. A model of a GaAs solar cell was constructed as shown in Figure 1. The thickness of the gold film was varied and a measurement of the transmittance of the gold film was made at the wavelength of the Carbon Dioxide laser used (10.6 μm). This was done to determine whether the gold coating would absorb a significant amount of the incident laser energy. The solar cell model was then constructed and irradiated with light from a CO_2 TEA laser. The impulse transmitted to the GaAs was measured as a function of time and of the thicknesses of the gold and SiO_2 film using a Sandia-type quartz gauge [Refs. 5 and 6]. Finally, an experiment was performed to determine the energy threshold for removal of the quartz film by the incident laser beam.

II. PREVIOUS WORK

The absorption of laser radiation by a great variety of materials under a large range of conditions has been examined by several experimenters. The type and mechanism of damage is dependent upon whether the target material is opaque or transparent to the incident laser light.

Damage to transparent materials by laser radiation has been the subject of much experimental and theoretical work. Observations of the damage itself are plentiful but a clear understanding of the mechanism of damage has yet to be developed.

The main mechanisms suggested for the laser-induced damage to transparent materials are [Ref. 7]:

a. Production of phonons (hypersound) in a stimulated Brillouin scattering process with the phonons being produced in an intensity sufficient to lead to a fracture of the material.

b. Absorption of light by defects in the material with resultant thermal shock and microplasma production. Using a ruby laser with 20 psec to 20 nsec pulse durations and depositing laser energy densities of from 3.5 joules/cm^2 to 16.0 joules/cm^2 on the target, Milam, et al. [Ref. 8] demonstrated that heating of inclusions ranging in size from 0.1 to 5.0 μm is the limiting mechanism for damage in TiO_2 and ZrO_2 films deposited on quartz substrates. A relationship

between the length of the laser pulse and the size of the inclusion heated was also developed. Short laser pulses can more easily heat small inclusions and long pulses preferentially heat large inclusions. It was shown by Hopper and Uhlmann [Ref. 9] that, in the first approximation, the inclusion that is most readily heated by a laser pulse of duration τ_p has a radius proportional to $(\tau_p)^{1/2}$.

c. The electron avalanche phenomenon. This phenomenon occurs at the surface of a transparent dielectric [Ref. 10]. "Free" electrons at the surface of the dielectric are accelerated by the electric field of the laser beam sufficiently to produce ionizing collisions with the atoms in the surface layer thereby producing more free electrons. When the lattice of the solid acquires energy from the free electrons so produced its temperature rises. The surface matter then melts, boils and evaporates, forming a partially ionized high-density vapor layer above the surface. This vapor layer absorbs laser light strongly and the absorbed light energy continues the ionization process. The mechanical damage resultant at the surface is primarily due to the plasma formed as a result of an optical discharge (thermal ionization of all the evaporated matter) and a shock wave generated by this discharge.

Damage produced in transparent materials by high-energy laser beams can range over a wide field of effects extending from microcracks or melted voids in the interior of the

material to craters and cracks on the surface of the material [Ref. 11].

The damage effects in transparent materials are highly power-dependent. If the incident laser radiation is below a certain power threshold, the laser beam passes through the material with no effect. However, if this threshold is exceeded, the laser beam is absorbed and damage of one form or another takes place [Refs. 12, 13 and 14]. For sodium chloride crystals irradiated with a Q-switched ruby laser this threshold occurs at 2.0 GW/cm^2; for Silicon Dioxide glass the threshold is at 470 GW/cm^2 [Ref. 12]. Wang [Ref. 14] has measured the damage threshold for copper reflectors irradiated with 10.6 μm radiation from a CO_2 TEA laser to be 150 MW/cm^2. Experiments [Ref. 11] have shown that the threshold for internal damage occurs at lower levels of irradiation than surface damage.

The absorption of laser energy by substances opaque to the wavelength of the laser used (absorbers) has also been the subject of considerable investigation. The variance of energy absorption with irradiance and duration of exposure shows three distinct regimes differing in the phenomena induced in the material by the laser beam.

The first of these regions is heating of the material without phase change. This results in a temperature rise in the material. This temperature rise may lead to simple thermal expansion of the material if the deposition of energy is slow enough. However, if the laser energy is deposited

rapidly enough, say in a time t comparable to or less than the time required for an elastic wave of velocity v to cross the area irradiated, a pressure wave can be generated. That is, if

$$t \leq a/v \tag{1}$$

where a is the radius of the area irradiated. In this case the irradiation takes place so quickly that the material remains "inertially clamped" during the absorption process. Hence, the volume of the irradiated portion of the material remains constant over the time immediately following the laser irradiation. A laser pulse of duration 10^{-8} sec. satisfies this condition [Ref. 15].

The next region considered is laser-induced melting of the target without vaporization. In this region the damage caused in the target consists of melting of target material to a depth dependent upon the power density of the laser beam irradiating the target and upon physical properties, such as the heat of fusion, of the target material. The optimum pulse length required for this effect ranges from 50 μsec to 5 msec and is much longer than the pulse lengths in the nanosecond range that were produced with the lasers used in the current investigation [Ref. 16].

The final region in which absorption by opaque materials takes place in laser-induced vaporization. For the purposes of the experiment performed this was the most significant

region. The strong energy fluxes concentrated over the small area of the focal spot of a laser beam produce such intense evaporation that significant pressures can be generated in the absorbing material by the recoil of matter ejected by evaporation [Refs. 17 and 18]. When the irradiation takes place in a vacuum a hot, dense plasma is formed above the material and the recoil of the particles in the plasma transfers momentum to the target. In an experiment in which aluminum targets were irradiated with a Neodymium-glass laser having an output between 4 and 11.5 joules, Krehl, Cooper and Schwirzke [Ref. 19] demonstrated that of the total mass ejected by the laser beam from the target about ten per cent was ionized and that this small ionized component was responsible for almost 80% of the momentum transferred to the target. A simple calculation by Askar'yan and Moroz [Ref. 17] shows that the recoil pressure of the ejected matter is many times the radiation pressure of the laser beam.

Pirri [Ref. 20] has developed a comprehensive theory for the momentum transfer to a surface from a laser-supported detonation wave initiated in the air above the target surface by a laser beam. Although this theory is not strictly applicable to the vacuum portion of the current investigation, it is described here in some detail as an excellent description of the mechanism of momentum transfer to a surface by a laser beam. The model is based upon the physical processes which occur when a high-power axisymmetric laser beam

interacts with a surface in the presence of an atmosphere. Figure 2 illustrates this model.

If τ_p is the laser pulse length, at some time $t << \tau_p$, on the order of 50 nsec, a laser-supported detonation wave is initiated above the target surface by breakdown of the small amount of surface material vaporized during this time. Once the detonation wave forms, the vaporization stops and the force delivered subsequently is a result of shocking the air above the surface to a high pressure.

This high pressure in the laser-shocked air means that there is a significant impulse delivered to the target after the laser pulse ends as the pressure relaxes to its ambient value. Hence, the dominant time scale for the momentum transfer process is τ_o, the time over which the impulse is delivered to the target surface rather than just the laser pulse length τ_p.

Initially, the flow of the hot, dense plasma from the surface is one-dimensional. At some later time, τ_{2D}, the flow becomes two-dimensional due to the thermal expansion of the plasma. This two-dimensional time is of the order of the time it takes the leading edge of the plasma to travel a laser spot diameter [Ref. 21]. This can be defined as

$$\tau_{2D} = \int_{o}^{D_s} dr/V \qquad (2)$$

where D_s is the diameter of the laser spot and V is the velocity of the leading edge of the plasma.

For the entire pressure-time history of the momentum transfer to be described by one-dimensional analysis the total time over which the impulse is delivered must be less than the two-dimensional time τ_{2D}. That is $\tau_p << \tau_{2D}$, $\tau_o \leq \tau_{2D}$.

In one dimension the detonation moves away from the surface with a velocity V_{DW}, given by

$$V_{DW} = [2(\gamma^2-1)E_o/\rho_o]^{1/3} \tag{3}$$

where γ is the ratio of specific heats of the air behind the detonation wave, E_o is the laser flux and ρ_o is the ambient density in front of the wave. The pressure behind the wave is

$$P_{DW} = \rho_o V_{DW}^2/(\gamma+1) \ . \tag{4}$$

The surface pressure on the surface while the laser is on and the flow is one-dimensional is

$$P_{SID} = [(\gamma+1)/2\gamma]^{2\gamma/(\gamma+1)} P_{DW} \tag{5}$$

The impulse per unit area at a point on the surface, I, is the sum of the contributions to the impulse transferred

while the laser is on and after the laser pulse has terminated. It is shown in later sections of this report that a one-dimensional analysis is justified for the conditions of the current investigation so only the case where $\tau_o \leq \tau_{2D}$ will be considered.

While the laser pulse is on, the impulse transferred to the surface is

$$I = \int_o^t p\,dt = P_{SID}\,t \qquad (0 \leq t \leq \tau_p) \qquad (6)$$

After the laser pulse is off the shock expansion flow field relaxes as a planar blast wave until τ_{2D} is reached. The pressure is then

$$P_s(t) = P_{sID}(\tau p/t)^{2/3} \qquad (\tau_p \leq t \leq \tau_{2D}) \qquad (7)$$

The impulse delivered to the surface is then

$$I = p_{S1D} + p_{S1D}\left(\frac{\tau_p}{t}\right) \int_0^t dt/t^{2/3}$$

$$= p_{S1D}\,\tau_p \{1+3[(p_{S1D}/p_{S(t)})^{1/2} - 1]\} \qquad (0 \leq t \leq \tau_{2D}) \qquad (8)$$

The total impulse is now obtained by setting $p_s(t)$ equal to p_o, the ambient pressure in front of the detonation wave.

Then, by substituting equations 3 through 5 into equation 8 and by assuming $p_{S1D} >> p_o$, it can be shown that

$$I = \left[6\left(\frac{\gamma+1}{2\gamma}\right)^{3\gamma/(\gamma-1)} \frac{(\gamma^2-1)}{(\gamma+1)^{3/2}}\right] \frac{\rho_o^{1/2} E_o \tau_p}{p_o^{1/2}} \sim \frac{E_o \tau_p}{V_o} \qquad (9)$$

for $\tau_o \leq \tau_{2D}$, where V_o is the ambient speed of sound. The impulse delivered to the surface is, therefore, proportional to the speed of sound in the ambient gas.

Experiments performed by Pirri, Schier and Northam [Ref. 22] showed the theory developed above to predict satisfactorily the momentum transfer to a surface irradiated with a high-power pulsed CO_2 laser in an average flux regime between 4 and 200 MW/cm^2.

Although Pirri's theory presents a comprehensive treatment of momentum transfer to a surface by a laser it is questionable whether it is completely applicable to the conditions used in this current investigation. According to Harrison [Ref. 23], in order for a laser-supported detonation wave to be formed laser power densities of the order of 10^5 to 10^8 watts/cm^2 are required in an atmosphere of pressures above 76 torr. Portions of the present investigation were carried out at pressures of the order of 10^{-5} torr. At these low pressures the impulse delivered to the target as a result of shocking the air above the target is not present. If this contribution to the total impulse is neglected, the impulse delivered to

the target is

$$I = p_{S1D} t \qquad (t \leq \tau_p) \tag{10}$$

This is just the expression for impulse per unit area delivered to a target in vacuum reported by Gregg and Thomas [Ref. 24].

A more suitable equation for predicting the maximum pressure developed in a target is given by Anderholm [Ref. 25]. Here the target is treated as a perfect gas bounded by material with acoustic impedance Z. The maximum pressure developed is

$$P_{MAX} = (ZE_o/3\tau_p)^{1/2} \tag{11}$$

where E_o is the laser energy density as before and τ_p is the laser pulse width. The acoustic impedance is given by

$$Z = \rho V_o \tag{12}$$

with ρ being the mass density and V_o the bulk sound velocity in the target. Verification of the maximum pressure predicted by this equation was obtained using a ruby laser to generate a pressure of 34 kbar in a quartz target. The value for maximum pressure of 29 kbar predicted by equation 11 agreed satisfactorily with the experimentally measured value.

Irradiation of opaque targets can generate very high pressures in the target. Several experiments have been performed by various authors to verify this fact. By irradiating a 0.66 mm thick aluminum target with a pulse of power density 2000 watts/cm^2 from a CO_2 laser, McMordie and Roberts [Ref. 26] measured pulses of up to 2 Bar. As noted above pressures in the kbar range were measured by Anderholm. By coating 1 mm thick targets with a water and paint coating and then irradiating the targets with light from a Q-switched Neodymium:glass laser with a laser fluence of 25 joules/cm^2, stresses in the kilobar ranges were measured by Fox [Ref. 27].

If the absorbing material is confined in some way, as in the experiment by Fox described above, the mechanism generating the stresses in the target is somewhat changed.

Confinement of the absorbing material between two transparent films causes a confined high-temperature plasma to be produced when the target is irradiated by a laser. This confined plasma drives a shock wave into the transparent media [Ref. 28]. The amplitude of this shock can be of the order of tens of kilobars.

Covering the absorbing material with a thin coating and then illuminating it with a high-power laser brings a different effect into play. The thin film is partially vaporized as a result of heating by thermal conduction from the laser-heated absorber surface. The resulting expansion

of gas and partial confinement at the absorber/thin film interface causes stress waves to be generated in the absorbing material [Ref. 29]. Experiments performed by Magee, Armistead and Krehl [Ref. 29] and by Fox [Ref. 27] have shown that the volatility of the coating has a significant effect upon the amplitude of the stress wave produced. Magee noted that as the curing time of the silver paint used as a coating for his targets was increased the magnitude of the stress waves produced in the target was reduced. This result was attributed to a change in the transmittance of the paint as its butyl acetate binder evaporated. In the experiment by Fox reported above [Ref. 26] it was observed that the coating of the target with a mere drop of water significantly increased the amplitude of the stress wave produced. For an aluminum target 0.17 mm thick it was noted that backface spallation occurred at laser fluences around 310 joules/cm^2 when the target was water-coated. For an uncoated target fluences of up to 500 joules/cm^2 produced no spallation. If the target was also coated with black paint, the threshold for backface spallation was further reduced to 200 joules/cm^2.

III. EXPERIMENTAL DESIGN

A. EQUIPMENT

A Carbon Dioxide (CO_2) Transverse Excitation at Atmospheric Pressure (TEA) laser was utilized throughout this experiment. A description of the laser is given by Strickland [Ref. 30], Behrens [Ref. 31] and Stevenson [Ref. 32]. The laser output was reflected off a 1 m focal length copper mirror through a germanium lens onto the solar cell model. The solar cell was, in turn, mounted in a test chamber that could be maintained either at atmospheric pressure or at a vacuum of 10^{-5} torr. depending upon the conditions desired. The solar cell model was mounted on a Sandia-type Quartz Pressure Gauge which enabled the pressure at the back face of the model to be monitored on a Tektronix 7704 oscilloscope. The energy output of the laser was monitored using a Ballistic Thermopile. A focal spot size of approximately 1.0 cm was maintained on the solar cell model by means of the germanium lens. A schematic of this experimental arrangement is shown in Figure 3.

1. CO_2 TEA Laser

The Naval Postgraduate School's CO_2 TEA Laser System consists of a resonant cavity, a Tachisto Marx-type generator, a passive electrical component pulse-shaping network, a direct current power source and a gas flow system.

The resonant cavity consists of a gas-filled lucite box constructed of 2.54 cm thick lucite, 101.6 cm long, 30.5 cm wide and 15.3 cm high, and two mirrors. At each end of the box a Sodium Chloride (NaCl) crystal is mounted to serve as a Brewster window. The back end of the resonant cavity is a 10.2 cm diameter polished copper mirror having a 3.0 m focal length. The front mirror is an 11.4 cm diameter plane parallel germanium mirror which transmits approximately 47% of the radiation striking it from inside the cavity, thus providing an outlet for the laser radiation.

Inside the lucite box is the electrode assembly which consists of a 2.0 cm thick aluminum plate located at the bottom of the box and a cathode assembly at the top. The plate is cut to fit the inside of the box and serves as the anode of the system. On the inside top of the box is the cathode. It is composed of 131 aluminum blades separated by lucite spacers and electrically connected by two threaded brass rods. The trigger assembly consists of 130 glass-encased nichrome wires set between the aluminum cathode plates with each wire set at the same height as the edge of the cathode blade. A gap of 5.8 cm is maintained between the anode wires and the anode plate [Ref. 32]. Some characteristics of the laser are given in Table I of Appendix A.

Selective excitation of the CO_2 upper laser level (the 001 level) in a TEA laser is collision dominated. An

electric discharge across the gap between the anode and cathode injects energy into the laser cavity which creates a uniform flux of electrons having an average energy of about one electron volt. A large number of inelastic collisions then take place between the CO_2 molecule in the ground state and the excited electrons. This causes the carbon dioxide molecule to be excited to various vibrational levels. Resonances exist in the carbon dioxide excitation cross-section for electron energies of 0.3, 0.6, and 0.9 electron volts. These resonances coincide with the vibrational ladder of energy levels of the carbon dioxide molecule and hence preferential excitation to these levels occurs. Thus an electron energy in the glow discharge near one electron volt excites the desired energy level ladder. Collisions between excited and unexcited carbon dioxide molecules thus populate the upper laser level very efficiently. The high efficiency arises because the energy levels are equally spaced and little energy is lost during transitions up or down the vibrational ladder. This high excitation efficiency, coupled with a quantum efficiency of about 41%, enables an operational efficiency of around 25% to be obtained. (Quantum efficiency is defined as the ratio of the laser photon energy to the upper level excitation energy.)

The presence of nitrogen (N_2) in the laser atmosphere provides a complementary excitation process. Nitrogen

molecules are also excited to a higher vibrational energy level by electron impact. The lowest excited vibrational energy levels of nitrogen and the upper laser level of the carbon dioxide molecule are closely matched so an efficient transfer of energy occurs through collision of excited nitrogen molecules with ground state carbon dioxide molecules.

Once a carbon dioxide molecule is selectively excited to the upper laser (001) level, it can emit a 10.6 μm photon as it decays, or is stimulated, to the lower laser level (010). It must be quickly removed from this level to maintain the population inversion necessary for lasing. This is accomplished by adding a light gas, such as Helium (He), with a collision rate much larger than carbon dioxide to the laser atmosphere to increase the rate of depopulation of the lower laser level to the ground state.

The NPS CO_2 laser is operated with an atmosphere of carbon dioxide, nitrogen and helium in a mixture of 90/5/5 per cent and at a flow rate of about one-half liter per second.

Conditions for lasing are induced by electrical breakdown between the cathode and anode located in the laser box. This produces the direct electron collision and molecule-molecule energy transfer process that results in the carbon dioxide population inversion. The laser is operated at atmospheric pressure rather than at low pressure in order to make use of the high molecular density and consequently greater energy available.

The electrical power required for excitation of the laser is produced by a three-stage Marx generator supplied with a positive power voltage of up to 22 kilovolts and 15 milliamperes by an unregulated d.c. power supply. Due to the voltage multiplication of the Marx generator voltages of up to 66 kilovolts can be generated across the laser electrodes. Pulse-shaping is required to obtain the uniform glow discharge needed for gas pumping. This is accomplished through the use of a network of passive circuit elements that controls the voltage rise time and decay time constants of the input energy and the Marx generator. This network is discussed in Ref. 31.

2. Solar Cell Model

Reference 33 describes the fabrication of a Gallium Arsenide Solar Cell. The Gallium Arsenide (GaAs) substrate is coated with a continuous platinum (Pt) film approximately 40 Angstroms thick to establish the barrier contact height. This platinum film is then overlaid with a gold (Au) contact several thousands of Angstroms thick. Since a gold layer of this thickness is essentially opaque to visible light, a large area solar cell such as is used on satellites, utilizes a grid structure for the gold contact layer. Such a grid structure is illustrated in Figure 4. The entire solar cell is then coated with an antireflective coating of silicon dioxide (SiO_2).

The model of the gallium arsenide solar cell constructed for the current investigation was designed to

approximate the cross-section of the cell at one of the grid lines. An illustration of this model is given in Figure 1. The model consisted of a gallium arsenide substrate approximately 3.0 mm thick and 1.0 cm in diameter. A gold film of thickness varying up to 5000 Angstroms was vacuum deposited on this substrate. A silicon dioxide film of thickness up to 3000 Angstroms was then deposited onto the gold film. The model was then mounted on a Sandia quartz gauge using a thin layer of epoxy cement.

Since the gold layer is thick enough so that all of the laser radiation incident upon it is absorbed, the momentum coupling between the gold and the platinum layers would be entirely mechanical. It [Ref. 34] has been stated that a film of thickness on the order of 50 Angstroms is invisible as far as mechanical coupling is concerned. Therefore the thin platinum film was not included on the solar cell model used in the current investigation.

3. Sandia Quartz Gauge

The piezoelectric quartz gauges used in this experiment were provided by Stanford Research Institute and were of the type developed by Graham [Ref. 5] at Sandia Laboratories. This type of pressure gauge has a resolution on the order of a few nanoseconds.

The operation of the gauge is based on the fact that when a force is applied on a piezoelectric crystal, such as quartz, it results in the formation of a stress

within the crystal that distorts the ionic structure of the crystal. This distortion results in an increase in the polarization of the sample.

It is well-known from electromagnetic theory that the electric displacement vector is given by

$$\vec{D} = \varepsilon\vec{E} + \vec{P} \tag{13}$$

where $\vec{P}$ is the piezoelectric polarization, $\vec{E}$ is the electric field and ε is the dielectric permittivity. If a one-dimensional strain is assumed, the piezoelectric equation becomes

$$D_x = Td_{21} + \varepsilon E \tag{14}$$

where T is the stress and d_{21} is the piezoelectric stress constant. If it is assumed that the piezoelectric polarization is directly proportional to the stress with a coefficient f that is independent of time and stress over a given stress range, P_x becomes

$$P_x = f\sigma_x(x) \tag{15}$$

where $\sigma_x(x)$ is the x-component of the stress. For an X-cut quartz crystal [Ref. 5]

$$d_{21} = 2.25 \cdot 10^{-12} \text{ coulomb/newton}$$

$$\varepsilon = 4.06 \cdot 10^{-11} \text{ farad/meter.}$$

For the static case, the open circuit voltage is given by [Ref. 35]

$$g = d_{21}/\varepsilon = 0.55\ \ell F/Tw \text{ (volt-meter/newton)} \qquad (16)$$

and the short-circuited charge for a given applied force is

$$Q = d_{21}\ F\ell/t \qquad (17)$$

where F is the applied force, considered positive for an extensional force, ℓ is the crystal length, w is the crystal width and t is the crystal thickness.

The development given above is adequate for low-frequency impulses. However, in the current investigation the analysis is complicated because the laser pulse produces a stress wave with a short wavelength.

Graham, et al. [Ref. 5] have analyzed the short-circuit piezoelectric current induced by a rapidly changing impulsive load applied to the quartz. This load propagates as a stress wave along the x-axis of a quartz disc. The displacement current generated by this stress wave is

$$i_D = A\ dD/dt \qquad (18)$$

where A is the electrical area of the disc and D is the displacement vector.

From equation 14 and assuming one-dimensional stress in the x-direction it is seen that

$$\int_0^{\ell} D_x(x)\, dx = \int_0^{\ell} P(x)\, dx + \varepsilon \int_0^{\ell} E_x(x)\, dx \qquad (19)$$

where ℓ is the thickness of the quartz disc.

Assuming a short circuit between the electrodes and that the crystal has a constant permittivity, the last integral in equation (19) becomes

$$\int_0^{\ell} \varepsilon E_x(x)\, dx = 0 \qquad (20)$$

The conductivity of the quartz is essentially zero, so

$$1/\ell \int_0^{\ell} P_x(x)\, dx = D_x \ . \qquad (21)$$

From equation 15 it is known that

$$P_x = f\sigma(x) \ .$$

If it is assumed that the quartz is linearly elastic it can be stated that

$$\sigma(x,t) = \sigma(x-u_s t) \tag{22}$$

where u_s is the wave propagation velocity. Therefore, from equation 18, we have

$$i_D = A\, d/dt\, [1/\ell \int_0^{\ell} f\sigma(x-u_s t)\, dx]$$

$$= -fu_s A/\ell \int_0^{\ell} \partial(\sigma x)/\partial x\, dx$$

$$= f\, u_s\, A\, (\sigma_o - \sigma_\rho)/\ell \tag{23}$$

where σ_o is the x-component stress at the input electrode and σ_ρ is the x-component at the rear electrode.

For times less than the time required for the stress wave to travel the length of the quartz, $\sigma_\rho = 0$ and

$$i_D = f\, A\, u_s\, \sigma_o/\ell\ . \tag{24}$$

Therefore, for times less than the wave transit time, the piezoelectric current generated in the quartz crystal is directly proportional to the stress generated in the quartz by the laser pulse. The gauge used in this investigation

has a time resolution on the order of a few nanoseconds and, using a 50 ohm shunt resistor, has a sensitivity of 1.09 mV/bar. The gauge is illustrated in Figure 5.

This gauge employed a guard ring configuration as described by Jones [Ref. 6] and illustrated in Figure 6. As is shown, the inner portion of the X-cut quartz disc is electrically isolated from the outer portion by separating the vapor-coated electrode into two regions. This guard ring configuration eliminates field distortions. At the outer edge of the disc, the discontinuity in electric potential and dielectric permitivity of the quartz produces electric field fringing analogous to that found in parallel-plate capacitors. The guard ring restricts observation to the central region of the quartz disc where there is negligible fringing.

This guard ring also aids in the elimination of distortions caused by unloading waves. As the stress wave propagates through the disc in the axial direction, boundary conditions generate shear and dilational waves immediately behind the wavefront at the lateral edge of the disc. These unloading waves then propagate laterally inward from the edge and the crystal is no longer in a state of one-dimensional strain. The central region of the disc will be one-dimensional only for the first wave transit time if the width of the center electrode is such that the unloading wave does not reach the central region during the first wave transit time.

For proper monitoring of the pressure pulse, the propagation time of the pressure pulse in the quartz must be larger than the half-width of the laser pulse. For the 250 ns pulse width of the CO_2 TEA laser and a speed of sound in quartz of 5700 meters per second, this requires that the gauges used in the CO_2 laser must have quartz discs at least 1.44 mm thick. The gauges used had quartz discs 3.0 mm thick so this requirement was satisfied.

Care also had to be taken that a pulse reflected at the rear of the gallium arsenide target sample did not reach the gauge during the loading phase. This required that the target sample thickness, d_s, had to satisfy [Ref. 29]

$$d_s \geq t_q \, v_s/2 \tag{25}$$

where t_q is the propagation time of a pressure (sound) pulse in the quartz plate and v_s is the speed of sound in the gallium arsenide. For a sound speed of 5000 meters per second in gallium arsenide and the 500 ns transit time in the quartz disc calculated from the data for quartz given above, this required that d_s be greater than 1.25 mm. The 3.0 mm thickness of the gallium arsenide samples used satisfied this requirement.

A final requirement for proper operation of the quartz gauge was that the stress be essentially uniaxial. To ensure this a laser spot diameter of slightly greater than the 1.0 cm diameter of the gallium arsenide sample was used throughout the experiment.

4. Ballistic Thermopile

The total energy output of the CO_2 TEA laser was monitored by directing the laser beam into a ballistic thermopile. The ballistic thermopile is a calorimetric device that measures the temperature rise due to absorbed radiation. It is composed of two nickel-plated cones (receiver and reference) and two series-connected iron-constantan thermocouples. These thermocouples are situated so that the hot junctions are attached to the receiver cone and the cold junctions to the reference cone. Radiant energy is directed into the receiver cone where it is almost totally absorbed. The temperature difference between the receiver cone and reference cone generates an emf, which is monitored by an externally connected microvoltmeter. The peak meter reading is linearly proportional to the total input energy with a constant of proportionality equal to 44.9 μV/joule. Due to the high reflectivity in the cone, the polished surface resists the destructive effects of the high peak power pulses found in laser plasma research. Some characteristics of the HADRON Ballistic Thermopile used in this investigation are given in Table II of Appendix A.

5. Test Chamber for CO_2 Laser System

The test chamber utilized was constructed of a rectangular aluminum block 11.4 cm long, 8.9 cm wide and 10.0 cm high through which a 6.4 cm diameter hole had been drilled from the top to the bottom. Five access ports were

provided, a 4.0 cm diameter port in each side and a 6.4 cm diameter port on the top of the chamber. An overhead view of the test chamber is shown in Figure 7.

Laser light was introduced into the chamber through Port A. Ports B and C were covered with plexiglass windows to enable the system to be placed under vacuum by means of a vacuum system connected at Port D. The test chamber was mounted on an aluminum bed plate and that was adjustable in height by means of bolts mounted at each corner of the plate.

B. THEORY

1. Determination of Peak Pressure in the Gallium Arsenide Substrate

Equation 10 provided a method whereby the maximum pressure developed in a transparent material by laser irradiation can be calculated. However, the problem presented by the generation of a pressure pulse in the GaAs layer of the solar cell model used in the current investigation is complicated by the fact that, although GaAs is essentially transparent to the 10.6 μm radiation used, the gold and silicon dioxide coatings are strongly absorbing at this wavelength. Also, the thickness of these two films was such that the incident laser radiation was totally absorbed prior to reaching the GaAs substrate. Hence the problem of predicting the magnitude of the pressure pulse in the GaAs was reduced to that of predicting the pressure

in the gold-silicon dioxide combination layer and then computing a correction factor for the mechanical coupling of the pressure pulse across the gold-gallium arsenide interface.

By consideration of the conservation of momentum across the interface between two materials of different acoustical properties Krehl, et al. [Ref. 19] developed an equation for this correction factor. Employing this result, the magnitude of the pressure in the gallium arsenide transmitted by the gold layer is

$$P_{Au} = P_{GaAs}(v_{GaAs}\rho_{GaAs} + v_{Au}\rho_{Au})/2\, v_{GaAs}\rho_{GaAs} \qquad (26)$$

where ρ is the initial density and v is the elastic wave velocity in the medium. Using the values of ρ and v for gallium arsenide and gold given in Table III of Appendix A we obtain

$$P_{GaAs}/P_{Au} = 0.43 \ . \qquad (27)$$

A similar correction must be made to the pressure measured by the quartz gauge to obtain the pressure in the gallium arsenide. In this case the correction factor was found to be

$$P_{GaAs}/P_{SiO_2} = 1.57 \qquad (27a)$$

Using equations 27 and 27a it is possible to obtain the true pressure generated in the gallium arsenide if the pressure in the gold layer or the pressure measured by the quartz gauge is known.

The problem of predicting the pressure generated in the gallium arsenide by the laser pulse is now reduced to predicting the pressure in the gold layer. From equation 11 it is known that

$$P_{Au} = (Z_{Au}E_o/3\tau_p)^{1/2} . \qquad (28)$$

But since the silicon dioxide layer covering the gold layer is an absorber of 10.6 μm radiation not all of the laser energy incident upon the silicon dioxide should be transmitted to the gold layer. However, from Table III of Appendix A, it is seen that the absorption coefficient of silicon dioxide at 10.6 μm is $3.0 \cdot 10^3$ cm^{-1}. For the silicon dioxide films with thicknesses on the order of thousands of Angstroms, such as those used in the current investigation, the energy fraction transmitted through the silicon dioxide layer is about 0.98. So virtually all of the incident energy is transmitted to the gold layer by the silicon dioxide layer and it can be stated that

$$E_{Au} = AE_o \qquad (29)$$

where A is the absorptance of the Au-SiO_2 film system. Equation 28 then becomes

$$P_{Au} = (Z_{Au} A E_o/3\tau_p)^{1/2} . \quad (30)$$

So if the laser energy density E_o and the absorptance A are known the pressure in the gallium arsenide can be calculated using equations 27 and 30.

2. Derivations of the Absorptance

Since both the gold and the silicon dioxide layers are absorbers of 10.6 μm radiation, the problem of finding the absorptance of the system is that of finding the absorptance of a single absorbing layer (the silicon dioxide) on an absorbing substrate (the gold). This problem has been solved by Heavens [Ref. 36].

The energy that is coupled into the system consists of the laser energy that is absorbed by the silicon dioxide layer and the laser energy that is transmitted through the silicon dioxide layer and is then absorbed by the gold layer. If the absorptance is defined as the ratio of the energy coupled into the system by both of these means to the incident energy, and the reflectance of the system is defined as the ratio of the energy reflected to the energy incident, then

$$A = 1-R \quad (31)$$

where R is the reflectance.

From Heavens, the reflectance of a system of thin films such as illustrated in Figure 6 is

$$R = cc^*/aa^* \tag{32}$$

where c and a are obtained from the matrix product of the matrices of Fresnel coefficients for the system. That is,

$$(C_1)(C_2)\ldots.(C_{n+1}) = \begin{pmatrix} a & b \\ c & d \end{pmatrix} . \tag{33}$$

In general, for an absorbing medium, the elements of the matrix of Fresnel coefficients are all complex and are given by

$$(C_m) = \begin{pmatrix} p_m + iq_m & r_m + is_m \\ t_m + iu_m & v_m + iw_m \end{pmatrix} \tag{34}$$

where

$$g_m = \frac{(n_{R_{m-1}}^2 + n_{I_{m-1}}^2 - n_{R_{m-1}}^2 - n_{I_{m-1}}^2)}{[(n_{R_{m-1}} + n_{R_m})^2 + (n_{I_{m-1}} + n_{I_m})^2]} \tag{35}$$

$$h_m = \frac{2(n_{R_{m-1}} n_{I_m} - n_{R_m} n_{I_{m-1}})}{[(n_{R_{m-1}} + n_{R_m})^2 + (n_{I_{m-1}} + n_{I_m})^2]} \tag{36}$$

$$\alpha_{m-1} = \frac{2\pi}{\lambda} n_{I_{m-1}} d_{m-1} \tag{37}$$

$$\gamma_{m-1} = \frac{2\pi}{\lambda} n_{R_{m-1}} d_{m-1} \tag{38}$$

in which n_R and n_I are the real and imaginary parts of the complex index of refraction for the material composing the layer and d is the thickness of the layer.

For normal incidence the quantities of equation 34 are defined by

$$p_m = e^{\alpha_{m-1}} \cos \gamma_{m-1} \tag{39}$$

$$q_m = e^{\alpha_{m-1}} \sin \gamma_{m-1} \tag{40}$$

$$r_m = e^{\alpha_{m-1}} (g_m \cos \gamma_{m-1} - h_m \sin \gamma_{m-1}) \tag{41}$$

$$s_m = e^{\alpha_{m-1}} (h_m \cos \gamma_{m-1} + g_m \sin \gamma_{m-1}) \tag{42}$$

$$t_m = e^{-\alpha_{m-1}}(g_m \cos \gamma_{m-1} + h_m \sin \gamma_{m-1}) \tag{43}$$

$$u_m = e^{-\alpha_{m-1}}(h_m \cos \gamma_{m-1} - g_m \sin \gamma_{m-1}) \tag{44}$$

$$v_m = e^{-\alpha_{m-1}} \cos \gamma_{m-1} \tag{45}$$

$$w_m = -e^{-\alpha_{m-1}} \sin \gamma_{m-1} \quad . \tag{46}$$

A double suffix notation can be adopted to denote the elements of the product matrices. Thus the elements of the single layer system under consideration are

$$(C_1)(C_2) = \begin{pmatrix} p_{12} + iq_{12} & r_{12} + is_{12} \\ t_{12} + iu_{12} & v_{12} + iw_{12} \end{pmatrix}$$

where

$$p_{12} = p_2 + g_1 t_2 - h_1 u_2 \tag{47}$$

$$q_{12} = q_2 + h_1 t_2 + g_1 u_2 \tag{48}$$

$$t_{12} = t_2 + g_1 p_2 - h_1 q_2 \tag{49}$$

$$u_{12} = h_2 + h_1 p_2 - g_1 q_2 \tag{50}$$

and the other terms of the product matrix are obtained in the same fashion as equations 47 through 50 by matrix multiplication of the individual matrices (c_m). From equation 32 and from the quantities defined in equations 35 through 50, the reflectance of the system is

$$R = (t_{12}^2 + u_{12}^2)/(p_{12}^2 + q_{12}^2) \tag{51}$$

The absorptance of the system can then be calculated from equation 31.

In general the quantities n_R and n_I needed to calculate the terms of equation 51 are wavelength dependent. Values for these quantities are tabulated in Table III of Appendix A for the wavelength of 10.6 μm used in the current investigation.

IV. EXPERIMENTAL PROCEDURE

A. MEASUREMENT OF PRESSURE PULSES

The magnitude of the pressure pulse at the backface of the gallium arsenide was monitored using the Sandia Quartz Gauge previously described. The output of the gauge was displayed on the screen of a Tektronix 7704 Oscilloscope and recorded photographically. Triggering for this oscilloscope was obtained from a Tektronix T-555 oscilloscope utilizing its delayed trigger capability. The T-555 oscilloscope was, in turn, triggered by the current output of the Marx bank of the Carbon Dioxide laser. Delays of up to 1.0 microsecond were used to allow for the delay between firing the Marx bank and initiation of the laser pulse. A schematic of the circuitry used is shown in Figure 8.

B. MEASUREMENT OF ENERGY DELIVERED TO TARGET

Prior to initiation of the experimental data runs the Carbon Dioxide laser was aligned so that its energy output at a given applied voltage varied less than ten per cent. After the data run was completed the energy output was measured using the ballistic thermopile to verify that no significant change in the laser output occurred. The experimental apparatus was such that continuous monitoring of the laser output was not practical.

Since the laser beam was required to pass through various optical components prior to irradiating the solar cell model not all of the energy of the laser pulse reached the target; some was absorbed by the various optical components.

The principal components that absorbed the laser energy were the germanium lens used to focus the laser beam and, in the case of the vacuum data runs, the window in the test chamber through which the laser light was admitted to the chamber.

An experiment was performed in which the energy output of the laser was measured with the ballistic thermopile both before and after the laser beam passed through the germanium lens. The lens was found to transmit about 90% of the laser energy.

A similar experiment was performed on the germanium window used as an entrance window for the vacuum data runs. However, as is described in the Experimental Results section of this report, the energy transmitted through the germanium window was a function of the number of laser shots. A transmittance curve was obtained for this window and is shown in Figure 9. A correction factor was then applied to the laser energy for the value appropriate to the laser shot.

From the above experiments a correction factor of 0.9 was applied to the laser energy to account for the absorptance of the lens and a correction factor corresponding to the transmittance of the window for a given laser shot was applied to account for the absorptance of the window.

V. EXPERIMENTAL RESULTS AND ANALYSIS

A. ENTRANCE WINDOW DAMAGE

An unexpected result that arose in the performance of the experiment was the inability to find a material for the entrance window to the test chamber that was capable of withstanding the power density of 10^7 watts/cm^2 needed to obtain the 1.0 cm spot diameter required on the solar cell model. Lack of a window that could withstand more than a few shots at this power density severely limited the amount and quality of the data obtained in the vacuum data runs.

Four different materials were tried in an attempt to find a suitable material: Sodium Chloride, Potassium Bromide, Zinc Selenide, both with and without an anti-reflective coating, and anti-reflective coated Germanium.

Of these materials the Potassium Bromide window showed damage in the form of a burn spot on the first shot and the Sodium Chloride and the anti-reflective coated Zinc Selenide windows showed similar damage after about three shots. Closer examination of the Zinc Selenide window showed indications of possible internal damage and spallation on its back face.

Since the anti-reflective coating on the window was damaged, it was decided to remove it and determine if the uncoated surface was better able to pass the laser beam without damage. It was found that this was not the case. After three shots, it was observed that further surface

damage was occurring and experimentation with this window was terminated.

Finally, an anti-reflective coated germanium window was obtained and was found to survive five shots without any apparent damage. A vacuum data run was then initiated using this window. However, after a few more shots surface damage was visible on the window and the run terminated.

A subsequent data run was made by irradiating a different portion of the window surface. In this run surface damage was observed after five shots.

Pictures of the damage caused to the Sodium Chloride and Germanium windows are included as Figures 10 and 11.

The primary cause of the damage observed in the window materials examined is felt to be that the incident power density exceeded the intrinsic threshold for damage of the material coupled with damage due to possible inclusions in the materials

The possibility that inclusions in the surface layer of the Sodium Chloride and Potassium Bromide windows were responsible for the damage to these windows is extremely plausible. These windows were polished by the experimenter and it is quite likely that small pieces of the polishing compound could have been imbedded in the surface of the windows. These particles could then have acted as strong absorbers for the incident 10.6 μm radiation.

The most probable mechanism to explain the damage observed in the Zinc Selenide and Germanium windows is

exceeding the intrinsic damage threshold for the anti-reflective coatings of these windows. While no information for the coating of the Zinc Selenide window was available, information given by the manufacturer of the Germanium window indicated that the damage threshold for the coating on this window was about 100 megawatts/cm^2. Measurement of the burn spot on the Germanium window indicated that it had a diameter of about 0.5 cm; this corresponds to a power density of about 7000 megawatts/cm^2, well in excess of the damage threshold of the coating.

B. PRESSURE PULSE MEASUREMENTS IN VACUUM

Two data runs were made under a vacuum of approximately 10^{-5} torr. using the germanium entrance window, a laser energy of 5.25 joules, and two different sets of thicknesses for the silicon dioxide and gold coatings of the solar cell model. Tables IV and V of Appendix A list the results for each set of film thicknesses. A graph of the natural logarithm of the peak pressure measured in the gallium arsenide versus shot number of the laser for each set of coating thicknesses is displayed in Figures 12 and 14.

As can be seen on these graphs, the peak pressure in each case steadily decreased from a high initial value to about 100 bars as the shot number increased. The duration of the pressure pulse in both cases remained approximately constant at about 400 ns until the last two shots when it shortened to around 250 ns. Figures 16 and 17

display early and final pressure pulses for the system of a 1000 Angstrom layer of silicon dioxide on a 1000 Angstrom layer of gold (1000/1000 system). Similar pulses for a 1000/2000 system are shown in Figures 18 and 19.

Observations of each gauge after completion of the data run revealed that in both cases the layers of silicon dioxide and gold had been removed from most of the surface of the gallium arsenide substrate. Since the duration of the data run for the thicker of the two systems (the 1000/2000 system) was the shorter (10 shots) it is concluded that it required an equal number of shots to remove the coatings from the 1000/1000 system.

C. PRESSURE PULSE MEASUREMENTS AT ATMOSPHERIC PRESSURE

Three data runs were made at atmospheric pressure using the following sets of gold and silicon dioxide layer thicknesses:

1. 1000/2000
2. 2000/3000
3. 0/5000

In the above sets the thickness of the silicon dioxide layer in Angstroms is followed by the thickness of the gold layer in Angstroms.

In all cases a laser energy output prior to any optical components of 5.25 joules was used and a spot diameter of 1.3 cm was maintained on the solar cell model. The data from these runs are tabulated in Tables VI and VII of Appendix A.

In the 1000/2000 system the peak pressure pulse in the gallium arsenide was initially 14.0 bars and decreased to a value of 9.0 bars after 13 shots and remained nearly constant at this value for the remaining six shots of the run. The duration of the pressure pulses measured remained nearly constant at 1.0 μsec. After six shots, damage to the coatings was observed in the form of total removal of the silicon dioxide and gold layers at various points on the surface of the solar cell model. Figure 20 displays a typical pulse for this system. Figure 21 displays a graph of the natural logarithm of peak pressure versus shot number for this data.

The second system examined at atmospheric pressure consisted of thicker coatings. In this case a 2000 Angstrom layer of silicon dioxide was deposited onto a 3000 Angstrom layer of gold. The results of the fourteen shots taken at this 2000/3000 system did not display the decrease in peak pressure observed in the previously described results. For this system the peak pressure measured remained nearly constant with an average value of 8.0 bars and displayed a mean pulse duration of approximately 600 nsec.

The greater thickness of the silicon dioxide coating allowed an observation to be made to obtain an estimate of the number of shots required to at least partially remove the silicon dioxide layer. It is estimated that the silicon dioxide layer was almost totally removed from the central portion of the surface of the solar cell model after only

one shot. After a total of six shots, gallium arsenide was visible at the center of the surface indicating that both the silicon dioxide and gold layers were removed. A typical pressure pulse measured for this system is shown in Figure 22. Figure 24 shows the surface of the solar cell model upon completion of fourteen shots.

A final series of shots was run on a target upon which a 5000 Angstrom layer of gold was deposited. No layer of silicon dioxide was deposited on this solar cell model in order that the effects of a thick layer of gold upon the pressure pulse generated could be examined. An initial peak pressure of approximately six bars was measured with a duration of approximately 2.0 μsec. This magnitude of the pressure pulse persisted for four shots and then the pulse was lost in the noise displayed on the screen of the oscilloscope. The run was terminated at eight shots with no damage to the gold surface apparent. Figure 23 shows a typical pulse from this series.

D. COMPUTER MODELING OF PEAK PRESSURE PULSE

A computer code was developed to predict both the peak pressure in vacuum and in atmosphere for a given set of silicon dioxide and gold layer thicknesses. For irradiation in vacuum the plasma tamping model presented by equation 30 was used and for irradiation at atmospheric pressure the laser-supported detonation wave model developed by Pirri and expressed by equation 10 was used.

In both models the resultant pressure is dependent upon the energy density delivered to the target. From equations 29 and 31 it can be seen that this energy density is at least partially dependent upon the reflectance of the target irradiated. Consequently, the computer code was designed to first calculate the reflectance of the solar cell model from equation 32, and from this to obtain the absorptance of the system from equation 31. The actual energy density delivered to the target was then calculated from equation 29. This resultant energy was then applied to equations 10 and 30 to obtain the expected magnitudes of the pressure pulses in vacuum and at atmospheric pressure respectively. For the case of the atmospheric measurements the duration of the pulse was measured from the photographic records of the data and this value was then assigned to the variable t in equation 10.

The code was also designed to examine the effects of reducing the thickness of the silicon dioxide and gold layers upon the peak pressure expected. Since the obvious dependence of the predicted pressure on the thickness of the coating layers is through the exponential terms of the absorptance, this was accomplished by stripping off the silicon dioxide and gold films in 50-Angstrom increments and monitoring the effect this had on the peak pressures predicted.

The results of running this computer code for the thicknesses of silicon dioxide and gold used for the data

runs of the current investigation are summarized in Table VIII of Appendix A. The computer code itself is given in Appendix F.

As is shown in this table, in all cases where a silicon dioxide layer was present the initial reflectance of the system was almost 99%. At the point where the entire silicon dioxide layer is removed, the reflectance is only reduced by about 1%. The value of the reflectance at this point corresponds to that of the uncoated gold layer, that is about 9%.

E. ANALYSIS OF EXPERIMENTAL RESULTS

1. Pressure Measurements in Vacuum

The data depicted in Figures 12 and 14 was fitted to a straight line using a linear regression computer code. This was done to test the hypothesis that the peak pressure measured had a functional dependence upon shot number of the form

$$P = P_o \, e^{kx}. \tag{52}$$

where k is some constant dependent upon the initial thicknesses of the components of the film system and x is the shot number. The linear regression analysis yielded a value for k, the peak pressure to be expected after the first shot of the laser and a correlation factor that was a measure of the degree to which the data fitted the assumed straight line.

Since the data obtained in the vacuum runs was complicated by the fact that the entrance window of the

chamber absorbed some portion of the laser energy that varied from shot to shot, the measured pressure was corrected for the fraction of energy absorbed by the window. This was accomplished by dividing the pressure for a given shot number by the square root of the transmittance of the germanium window for that shot number. The factor $T^{1/2}$ was chosen since the energy transmitted through the window is TE_o' where E_o' is the energy incident on the window. The plasma tamping model used for predicting the pressure in vacuum is expressed by equation 30 wherein the energy density enters to the one-half power; hence the correction factor $T^{1/2}$ is applied.

Dividing by this factor has the effect of normalizing all the pressures to the values that would have been measured had the window not been present. A check to see if the only effect the absorption of energy by the window was to lower the pressure measured by comparing the value of k calculated by fitting a straight line to this "corrected" data with that obtained by analysis of the uncorrected data. Figures 12 and 14 display a graph of these corrected pressures versus shot number. If the values for k were equal or nearly so then the dependence of the peak pressure upon film thickness was independent of the energy absorption by the window.

For the 1000/1000 system the analysis yielded a value of k equal to -0.14 before the correction for the window was applied; after the correction was applied k was equal

to -0.13. For the 1000/2000 system the uncorrected value of k was -0.15 and after correction was -0.15. Based on the good agreement between the values of k before and after the correction was applied, the assumption that the energy absorption by the window was not dependent upon the thickness of the films was considered justified.

To determine the validity of the hypothesis of the functional relationship between shot number and peak pressure indicated by equation 52, the correlation factor calculated by the linear regression code was examined. In the case of the 1000/1000 system a correlation of 0.79 was calculated. For the 1000/2000 system the correlation factor was 0.89. Since a correlation of 1.0 indicates a perfect straight line, the values obtained indicated that the functional dependence assumed in equation 52 was possibly justified.

However, the correlation value of 0.79 calculated for the 1000/1000 system seemed to indicate that the functional relationship between peak pressure and shot number of equation 52 was not entirely correct. Closer examination of the data for the 1000/1000 system displayed in Figure 11 indicated that the peak pressure measured remained relatively constant from shot 10 on. Consequently, a functional relationship of the form

$$P = \overline{P} + P_o e^{k'x} \tag{53}$$

where k' was assumed to be thickness dependent was assumed for the first nine shots of the 1000/1000 and 1000/2000 systems. After nine shots it was presupposed that the pressure saturated to $\bar{P}$, the average pressure measured for shots 10 through 16 of the 100/100 system. Since the data for the 1000/2000 system covered only ten shots it was not possible to determine a corresponding value of $\bar{P}$ for that system and the value for the 1000/1000 system was also used for the 1000/2000 system.

To verify the relationship suggested by equation 53 the mean value of the pressures measured for shots ten through sixteen of the 1000/1000 system was calculated and found to be 215 bar. This value was then subtracted from P, the value of peak pressure after correction for the absorptance of the germanium window, corresponding to each shot number for the results of the vacuum data runs. The results of this subtraction are displayed in Tables IX and X of Appendix A. A graph of the natural logarithm of the resultant pressure P' versus shot number was then made. These graphs are shown as Figures 13 and 15. A linear regression analysis was performed on these data to test the validity of the relationship

$$P' = (P - \bar{P}) = P_o e^{k'x} \tag{54}$$

suggested by equation 53 for the first nine shots.

For the 1000/1000 system a value of k' of -0.44 and a correlation of 0.91 were obtained. The corresponding results for the 1000/2000 system were k' = -0.22 and a correlation of 0.85. Comparing these correlations to those reported above for the verification of equation 52 it is seen that, in the case of the 1000/1000 system, the correlation increased significantly. For the other system considered, the 1000/2000 system, the correlation did not change appreciably.

Viewing the fact that equation 54 yielded a higher correlation for the 1000/1000 system than did equation 52 and that the results for the 1000/2000 system did not appreciably change, it was concluded that the relationship between shot number and pressure generated is of the form of equation 54. That is, a "saturated" exponential for the first nine shots and a constant value thereafter. The saturation is felt to occur when the gold and silicon dioxide coating are entirely removed.

An assumption was made that the value of k in equation 52 and k' in equation 54 are dependent upon the initial thicknesses of the silicon dioxide and gold films of the solar cell model. An attempt to at least partially justify this assumption was made using the previously described computer code.

If the relationship between peak pressure and film thickness exists and is of the form of equation 54, that is,

a saturated exponential dependent upon the initial thicknesses of the gold and silicon dioxide films, the dependence will appear in the absorptance of the system since that is the only place where the film thicknesses appear. If there is a relationship between the constant k' in equation 54 and the initial thicknesses of the films then the pressure predicted by the plasma tamping model should equal that measured after the first shot of the laser.

The initial pressures measured for the film systems used (as predicted after the data had been analyzed by the linear regression) were:

1. 1000/1000 system: 1706 bar.
2. 1000/2000 system: 753 bar.

The values predicted using equation 30 were:

1. 1000/1000 system: 556 bar.
2. 1000/2000 system: 556 bar.

The predicted value for each case is respectively 33% and 74% of the measured value. Hence, it is concluded that there is at least some justification to the assumed relationship between film thickness and the proportionality constant k' of equation 54. The existence of this relationship would then imply that the decrease in peak pressure measured for successive shots can be attributed to the removal of the gold and silicon dioxide films by successive shots. Unfortunately, the computer model did not predict this decrease.

2. Pressure Measurements at Atmospheric Pressure

As has been previously described the measurements of pressure pulses generated at atmospheric pressure were of small amplitude. These results were as expected since previous work by Magee and others [Ref. 29] noted that in comparison to pressure pulses measured in vacuum, pressure pulses measured in atmosphere on identical targets were significantly smaller.

In the atmosphere measurements performed in the current investigation the pulses measured were generally of less than 10 bars magnitude. In only one case, the 1000/2000 system was there any variation of the pressure measured with shot number. The pressures measured on the thicker films, namely the 2000/3000 system and the 0/5000 system, remained almost constant throughout the data run with average values of 7.4 and 5.4 bars respectively.

For the data from the 1000/2000 system a linear regression analysis identical to that performed on the data from the vacuum cases was performed. However, no corrections were necessary for absorption by the entrance window since none was used. The linear regression analysis yielded a value of k equal to -0.046 and a correlation to the exponential relation between pressure and shot number of 0.87. This indicates that while an exponential relationship between shot number and pressure probably exists, is is a rather weak relationship, much weaker than that for the vacuum case.

The laser-supported detonation wave model for the generation of the pressure pulse leading to equation 10 was used to attempt to predict the pressure pulse using the experimenter-generated computer code previously discussed. The results were uniformly dismal. Comparison of the values tabulated in Tables VI, VII, and VIII show that the predicted pressures were consistently at least two orders of magnitude smaller than the experimentally measured pulses.

VI. CONCLUSIONS

A. DEPENDENCE OF PRESSURE UPON SHOT NUMBER AND FILM THICKNESS

Analysis of the curves of pressure versus shot number shown in Figures 13, 15 and 21 indicates that there exists an exponential relationship between the pressure generated and the shot number. Since total removal of the silicon dioxide and gold films covering the gallium arsenide substrate of the solar cell model was noted at some point during the data runs it is concluded that there exists some relationship between the peak pressure generated and the remaining thickness of the thin layers of silicon dioxide and gold remaining on the gallium arsenide substrate. The fact that the gallium arsenide substrate was entirely exposed at some points after only six shots on the 1000/2000 system at atmospheric pressure and that after this exposure was noted the pressure generated remained relatively constant seems to validate this conclusion. It is unfortunate that no similar observations could be made during the vacuum cases but the position of the solar cell model in the test chamber and the opacity of germanium to visible light precluded observation of the damage to the target until completion of the data run.

B. DETERMINATION OF THE PRESSURE GENERATION MECHANISM

The primary methods used to attempt to ascertain the mechanism whereby the observed pressure pulses were generated were examination of the duration of the measured pulse and a comparison of the measured pulse magnitude with that predicted by whichever of the two models considered in the previous sections of this report was applicable to the conditions of the particular experiment.

The comparison of the initial pressure pulses measured in vacuum to those predicted by the plasma tamping model of equation 30 yielded reasonable agreement between the observed and predicted pulse amplitudes. However, the consistent underestimation of the pulse amplitude by equation 30 indicates that some other mechanism may possibly be contributing significantly to the generation of the pressure pulses.

In an attempt to determine what this possible alternative mechanism might be an examination of the duration of the measured pressure pulse was made. In general, the duration of the pulses remained near 400 nanoseconds. This is about one and one-half the duration of the 250-nanosecond pulse of the Carbon Dioxide laser used to irradiate the solar cell model. Yang [Ref. 28] has reported that the pressure pulse is expected to have a duration close to that of the irradiating laser for pressure pulses generated by plasma tamping. This fact gave strong indication that possibly some other mechanism than plasma tamping might be the dominant mechanism.

A further indication to this effect is the requirement that power densities on the order of 10^9 watts/cm^2 are needed for plasma production [Ref. 41]. The power density used throughout the current investigation was of the order of 10^7 watts/cm^2, much lower than the power density needed for plasma production. This strongly suggested that a plasma was not being formed by laser irradiation of the target, thereby strongly suggesting that the plasma tamping model was not wholly applicable to the conditions of the experiment.

Based on these two observations the plasma tamping model was discarded as the chief mechanism for pressure generation in vacuum under the conditions of the current investigation.

The applicability of the laser-supported detonation wave model was not considered in the vacuum case since the formation of such a detonation wave required pressures far in excess of the 10^{-5} torr. pressure used in the vacuum measurements. This model was examined as a possible mechanism for the results obtained at atmospheric pressure but again the fact that the power density needed for plasma production was not met forced its exclusion as a possible mechanism. Also, the uniformly poor prediction of the model in the computer code would have forced its discard regardless of whether or not the conditions for plasma production were met.

The final mechanism examined as a possible explanation of the pressure pulse generation was the thermomechanical mechanism described by Ready [Ref. 42]. This mechanism

appeared attractive since it did not require removal of material from the target or the formation of a plasma. All that is required is rapid enough heating of an absorbing medium to cause the thermal expansion which generates the pressure wave. The mechanism suggests that the duration of the pressure wave generated is not tied to the laser pulse length but to the time required for the absorbing medium to thermally expand to its greatest extent and than to relax to its ambient thickness. In general, this time would probably be much longer than the laser pulse.

The strong possibility that this mechanism is the dominant mechanism in the current investigation is supported by two factors. The first is the long duration of the pressure pulse when compared to that of the laser pulse and the second is that the pressure pulse measured for the very thick 0.5000 system was of much smaller amplitude and greater duration than those measured for the thinner 1000/2000 and 1000/1000 systems. This small amplitude and long duration is attributed to the ability of the thick film to absorb and dissipate the thermal expansion over a much greater thickness than the thin film. This accounts for the long duration of the pressure pulse for the thick film since it takes a longer time for the thick film to expand than for a thin one.

C. DETERMINATION OF POWER THRESHOLD FOR REMOVAL OF COVERING FILMS

In all cases except the 0/5000 system, the layers of silicon dioxide and gold were found to have been rapidly removed by the relatively low power density of 10^7 watts/cm^2 used throughout the current investigation. In the cases where observation was made of the number of shots necessary for this complete removal to occur, the atmospheric irradiations, it was observed that no more than six shots were required before gallium arsenide was visible at some point on the surface of the solar cell model.

If the dominant mechanism at work is the thermomechanical mechanism described in the previous section, this removal of the films of gold and silicon dioxide is attributed to spallation. A portion of the pressure wave generated by thermal expansion of the gold layer is reflected at the gold-gallium arsenide interface and is of sufficient magnitude to exceed the strength of the bond holding the silicon dioxide to the gold thereby causing spalling of the silicon dioxide layer. A similar sequence of reflected waves could account for the removal of the gold coating. It should be noted that this explanation for the removal of the covering films was not verified by experimental work during the current investigation but is merely offered as a possible hypothesis to explain the film removal.

D. SUMMARY OF RESULTS

The main conclusions arrived at in the examination of the results of the current investigation are:

1. For films of gold less than 5000 Angstroms thick, there is a relationship between the pressure generated and the shot number of the form

$$P = P_o \, d^{k'x} + \bar{P} \, .$$

The value of k' is larger in vacuum than for irradiation at atmospheric pressure and the value of $\bar{P}$ in atmosphere is probably very much smaller than the corresponding value in vacuum. Since removal of the gold and silicon dioxide layers was observed after a series of shots, a dependence of the constant k' upon the initial thicknesses of the films is indicated.

2. The principal mechanism for the generation of the pressure pulses observed is apparently thermomechanical and due to thermal expansion of the gold layer.

3. The coatings of silicon dioxide used as an anti-reflective coating on the solar cell model are highly vulnerable to irradiation by a Carbon Dioxide laser even at the low power density of 10^7 watts/cm^2 used in the current investigation. However, this vulnerability may be significantly reduced by making the thickness of this layer much greater. The small amount of data obtained for the

irradiation of a 5000 Angstrom thick gold layer indicates that the contact grid composed of a gold layer of this thickness is able to absorb power densities on the order of 10^7 watts/cm^2 without damage.

VII. RECOMMENDATIONS FOR FURTHER RESEARCH

Several additional lines of investigation on the effects of laser irradiation on solar cells are indicated by the results of the current investigation. The first of these areas is verification of the results reported herein. These conclusions were based on a very small data base and hence are more indications of trends rather than fully justified arguments. However, before this can be done the experimental apparatus requires modification in some way to permit data to be taken under vacuum conditions without destruction of the entrance window to the test chamber. Also, several other sets of film thicknesses should be examined since the current investigation shows that the 1000 and 2000 Angstrom thicknesses of silicon dioxide are too thin to have a significant effect on the pressure generating mechanism.

Another possible area of investigation would be an attempt to time-resolve the pressure pulse generated, particularly to determine its time of onset and to attempt to resolve the contributions of each layer coating the gallium arsenide to the total pressure pulse measured.

Finally, since the results of this experiment seem to indicate thermomechanical generation of the pressure wave, investigation should be conducted to verify that this is indeed the mechanism operating. A refinement of the

computer model used in the current investigation to accomplish this is indicated. Also an attempt to predict the pressure pulse as a function of time should be attempted utilizing the material presented in Appendix C.

APPENDIX A

TABLES

TABLE I

NPS CO_2 TEA Laser Characteristics

Energy	up to 18 joules[a]
Pulse Width	250 nanoseconds[b]
Peak Output Power	up to 25 megawatts[a]
Wavelength	10.6 μm
Beam Shape	square, 4.5 cm x 4.5 cm[c]
Marx Input Voltage	66 kilovolt
Laser Efficiency	5% minimum

a. Only 14.4 joules have been produced with a peak power of about 21 Megawatt.

b. Considers only electron produced peak.

c. Unfocused, 75 cm from output mirror.

TABLE II

HADRON Ballistic Thermopile

Ballistic Time Constant	50 seconds
Equivalent Noise Level	300 microjoules
Maximum Energy Input	1000 joules
Maximum Power Input	10^9 watts
Sensitivity	44.9 microvolts/joule

TABLE III

Physical Constants at 10.6 micrometers

Material	ρ (gm/cm^3)	v_s (cm/sec)	n_R	n_I	k (cm^{-1})
GaAs	5.37	$5 \cdot 10^5$	3.07[a]	$8.8 \cdot 10^{-7}$[a]	$1.0 \cdot 10^{-2}$[b]
SiO_2	2.2	$5.7 \cdot 10^5$	1.46	0.25[b]	$3.0 \cdot 10^3$[b]
Au	19.3	$5.0 \cdot 10^5$	74.2	132.3	$1.5 \cdot 10^6$[b]

a. Reference 37.

b. Calculated; see Appendix B.

TABLE IV

Results for Data Run in Vacuum for
a 1000 A Layer of SiO_2 on a 1000 A of Au

Shot Number	Peak Pressure (bar)		Pulse Length (nsec.)
	Uncorrected	Corrected	
1	--	--	--
2	1440	2100	400
3	518	1016	300
4	232	485	400
5	--	--	--
6	144	301	240
7	217	452	400
8	144	301	400
9	130	272	340
10	80	166	320
11	97	203	400
12	97	203	400
13	--	--	--
14	130	272	300
15	115	239	280
16	100	209	320

TABLE V

Results for Data Run in Vacuum for a 1000 A Layer of SiO_2 on a 2000 A Layer of Au

Shot Number	Peak Pressure (bar)		Pulse Length (nsec.)
	Uncorrected	Corrected	
1	--	--	480
2	462	764	440
3	406	791	440
4	317	661	440
5	231	482	400
6	289	444	440
7	--	--	--
8	259	540	320
9	144	301	240
10	115	239	280

TABLE VI

Results for Data Run in Atmosphere for

a 1000 A Layer of SiO_2 on a 2000 A Layer of Au

Shot Number	Peak Pressure (bar)	Pulse Length (nsec.)
1	--	--
2	14	500
3	13	600
4	--	--
5	--	--
6	--	--
7	14	500
8	14	500
9	12	--
10	--	--
11	--	--
12	--	--
13	12	600
14	9	600
15	9	600
16	9	500
17	7	500
18	6	500
19	9	500

TABLE VII

Summary of Results for 2000/3000 and 0/5000 Systems at Atmospheric Pressure

System	Total Number of Shots	Mean Peak Pressure (Bar)	Mean Pulse Length (nsec.)
2000/3000	14	8.0	600
0/500[a]	7	5.4	2000

a. Pressure pulses for this system were of such small amplitude that it was extremely difficult to separate them from system noise. Therefore, the peak pressure and pulse duration upon which these mean values are based are, at best, estimates of true values.

TABLE VIII

System	Initial Reflectance[a]	Initial Peak Pressure in Vacuum (Bar)[b]	Initial Peak Pressure in Atmosphere (Bar)[3]	% Change in Reflectance
1000/1000	0.9869	488	0.8	-1.1
1000/2000	0.9869	488	0.8	-1.1
2000/3000	0.9851	592	0.3	-1.1
0/5000	0.9757	1258	1.5	--

a. Recall A = 1 - R.

b. As calculated by equation 30.

c. As calculated by equation 10.

d. Reflects change in reflectance when entire silicon dioxide layer has been removed.

TABLE IX

Peak Pressure for 1000/1000 System in Vacuum Corrected for an Average Saturation Pressure of 215 Bar.

Shot Number	Saturated Peak Pressure (Bar)	Peak Pressure Corrected for Saturation (Bar)
1	--	--
2	2100	1885
3	1016	801
4	485	270
5	--	--
6	301	86
7	452	237
8	301	86
9	272	57

TABLE X

Peak Pressure for 1000/2000 System in Vacuum Corrected for an Average Saturation Pressure of 215 Bar

Shot Number	Saturated Peak Pressure (Bar)	Peak Pressure Corrected for Saturation (bar)
1	--	--
2	764	549
3	791	576
4	661	446
5	482	267
6	444	229
7	--	--
8	540	325
9	301	86

APPENDIX B

Calculation of Values of n_R, n_I and k for Gallium Arsenide, Gold and Silicon Dioxide

From Ref. 43 the values of the real and imaginary parts of the index of refraction are given by

$$n_R = \left(\frac{\gamma+\beta}{2}\right)^{1/2} \tag{B-1}$$

$$n_I = \left(\frac{\gamma-\beta}{2}\right)^{1/2} \tag{B-2}$$

where

$$\beta = 1-\left(\omega_p^2/(\omega^2+\omega_c^2)\right) \tag{B-3}$$

$$\gamma = [\beta^2+(1-\beta)^2(\nu_c/\omega)^2]^{1/2} \tag{B-4}$$

in which ω is the laser angular frequency, ω_p is the plasma frequency given by

$$\omega_p = [4\pi e^2 N_e/m]^{1/2}$$

$$= 8.5\ (\rho z)^{1/2}\cdot 10^{15}\ \text{(radians/sec)} \tag{B-5}$$

where ρ is the density and z is the number of free electrons per atom.

The quantity ν_c is the collision frequency and is given by

$$\nu_c = \omega_p^2/4\pi\sigma_o \qquad \text{(B-6)}$$

in which σ_o is the static conductivity.

The absorption coefficient, k, is defined by

$$k = (2\omega/c)n_I \qquad \text{(B-7)}$$

where c is the speed of light in vacuum ($3.0 \cdot 10^{10}$ cm/sec).

The "skin depth" is defined by

$$\delta = k^{-1} = \lambda_o/4\pi n_I \ . \qquad \text{(B-8)}$$

For the CO_2 laser, λ_o = 10.6 μm and $\omega = 1.78 \cdot 10^{14}$ radians/sec^{-1}.

The transmittance, the ratio of transmitted to incident energy, is defined by

$$T = e^{-kx} \qquad \text{(B-9)}$$

where x is the thickness of the sample.

1. Calculation of n_R, n_I and k for gold.

For gold z = 1 and $\sigma_o = 3.7 \cdot 10^{17}$ sec^{-1} [Ref. 37].

Then

$$\omega_p = 8.4\ (\rho z)^{1/2} \cdot 10^{15}\ sec^{-1}$$

$$= 3.7 \cdot 10^{16}\ radians/sec^{-1}$$

$$\nu_c = \omega_p^2 / 4\pi\sigma_o$$

$$= 2.9 \cdot 10^{14}\ sec^{-1}$$

Then, substituting ω_p and ν_c into equations B-3 and B-4, it follows

$$\beta = 1 - (\omega_p^2/(\omega^2 + \nu_c^2))^2$$

$$= -1.2 \cdot 10^4$$

and

$$\gamma = [\beta^2 + (1-\beta)^2\ (\nu_c/\delta)^2]^{1/2}$$

$$= 2.3 \cdot 10^4\ .$$

Substituting these quantities into equations B-1 and B-2, the values for the real and imaginary parts of the index of refraction are

$$n_R = 74.2$$

$$n_I = 132.3$$

From equation B-7, the value of the absorption coefficient for gold is calculated to be $k = 1.5 \cdot 10^6$ cm^{-1}.

2. Calculation for n_I and k for silicon dioxide.

Reference 53 shows the transmittance of silicon dioxide at 10.6μm to be 0.82 for a sample 6680 A thick. From equation B-9, it is known that

$$T = e^{-kx} .$$

Then

$$\ln T = -kx$$

and

$$k = -\ln T/x . \qquad \text{(B-10)}$$

From the parameters given in Ref. 53,

$$k = 3.0 \cdot 10^3 \text{ cm}^{-1} .$$

From equation B-7, n_I is found to be

$$n_I = 0.25 .$$

3. Calculation of Absorption Coefficient for Gallium Arsenide.

From equation B-7, it is known that

$$k = (2\omega/c)n_I \ .$$

Table III of Appendix A shows that at 10.6 μm $n_I = 8.8 \cdot 10^{-7}$. Therefore $k = 1.0 \cdot 10^{-2}$ cm^{-1}. Note that this gives a skin depth of about 1.0 meter indicating that gallium arsenide is essentially transparent to the radiation from a CO_2 laser.

APPENDIX C

Development of Stress ($\sigma(x,t)$) and Temperature ($T(x,t)$) as Functions of Position, x, and time, t

An attempt was made to calculate the stress generated in the solar cell model as a function of the distance the stress has propagated into the model, x, and the time elapsed, t.

Michaels [Ref. 39] has solved for the stress generated in a bar as a function of x and t.

For an elemental slab of a bar of cross-sectional area A, the net force acting on the slab is

$$A\partial\sigma/\partial x\, dx = \rho A\, dx\partial^2 u/\partial t^2 \qquad \text{(C-1)}$$

in one dimension where

u = longitudinal displacement of slab,

t = time,

x = longitudinal coordinate of bar,

ρ = mass density of bar,

σ = longitudinal stress generated in bar.

In order for a one-dimensional treatment of the problem to be justified the effects of lateral inertia and shear must be negligible. The laser spot size used in the current investigation irradiated the entire surface of the

target so that the effects of lateral inertia and shear can be neglected.

From thermo-elasticity

$$\sigma = E(\varepsilon - \alpha T(x,t)) \qquad \text{(C-2)}$$

where

E = elastic modulus in dynes/cm^2,

α = coefficient of expansion in cm/cm $^\circ$K,

T = temperature of bar,

ε = total longitudinal strain.

Since

$$\varepsilon = \partial u/\partial x$$

and $c^2 = E/\rho$ where c is the stress wave velocity, equation C-1 becomes

$$\partial^2 u/\partial x^2 - \alpha \partial T(x,t)/\partial x = 1/c^2 \partial^2 u/\partial t^2 \ . \qquad \text{(C-3)}$$

For a finite bar extending from 0 to L, we have the boundary conditions that the stress at each end of the bar is zero. That is

$$\sigma\Big|_{\substack{x=0 \\ x=L}} = E[\partial u/\partial x - \alpha T(x,t)]_{\substack{x=0 \\ x=L}} = 0 \qquad \text{(C-4)}$$

or

$$\partial u/\partial x|_{x=0} = \alpha T(0,t) \qquad \text{(C-5)}$$

$$\partial u/\partial x|_{x=L} = \alpha T(L,t) \qquad \text{(C-6)}$$

The initial conditions for the bar are

$$u|_{t=0} = 0 \quad \text{and} \quad \partial u/\partial t|_{t=0} = 0$$

Recall equation C-3. Taking its finite Fourier cosine transform

$$1/c^2 \partial^2/\partial t^2 \int_0^L u(x,t) \cos(n\pi x/L)\, dx$$

$$= \int_0^L \partial^2 u/\partial x^2 \cos(n\pi x/L)\, dx$$

$$- \alpha \int_0^L \partial T(x,t)/\partial x \cos(n\pi x/L)\, dx \qquad \text{(C-7)}$$

Integrating the first term on the right-hand side of this equation by parts, the result is

$$\int_0^L \partial^2 u/\partial x^2 \cos\left(\frac{n\pi x}{L}\right) dx = (-1)^n [\partial u/\partial x]_{x=L} - [\partial u/\partial x]_{x=0}$$

$$- \frac{n^2\pi^2}{L^2} \int_0^L u(x,t) \cos\left(\frac{n\pi x}{L}\right) dx$$

Invoking the boundary conditions, equations C-5 and C-6, this becomes

$$\int_0^L \partial^2 u/\partial x^2 \cos\left(\frac{n\pi x}{L}\right) dx = (-1)^n \alpha T(L,t) - \alpha T(0,t)$$

$$- \frac{n^2\pi^2}{L^2} \int_0^L u(x,t) \cos\left(\frac{n\pi x}{L}\right) dx \qquad \text{(C-8)}$$

Using equations C-5, C-6 and C-8 equation C-7 becomes

$$1/c^2 \, \partial^2 \bar{u}_c(n,t)/\partial t^2 = (-1)^n \alpha T(L,t) - \alpha T(0,t)$$

$$- n^2\pi^2/L^2 \bar{u}_c(n,t) - \alpha \bar{\theta}_c(n,t) \qquad \text{(C-9)}$$

where

$$\bar{u}_c(n,t) = \int_0^L u(x,t) \cos(n\pi x/L) \, dx \qquad \text{(C-10)}$$

and

$$\bar{\theta}_c(n,t) = \int_0^L \partial T(x,t)/\partial x \cos(n\pi x/L) \, dx \qquad \text{(C-11)}$$

Equation C-9 reduces to

$$\partial^2 \bar{u}_c(n,t)/\partial t^2 + (n^2\pi^2c^2/L^2)\bar{u}_c(n,t) = c^2\alpha[(-1)^n T(L,t) - T(0,t)$$

$$- \bar{\theta}_c(n,t)] \qquad \text{(C-12)}$$

Now, define

$$\omega^2 = n^2\pi^2c^2/L^2 \quad \text{and}$$

$$P(n,t) = c^2\alpha[(-1)^n T(L,t) - T(0,t) - \bar{\theta}_c(n,t)]$$

and equation C-12 becomes

$$\partial^2 \bar{u}_c / \partial t^2 + \omega^2 u_c = P(n,t) \qquad \text{(C-13)}$$

The solution to this differential equation is [Ref. 39]

$$\bar{u}_c(n,t) = 1/\omega \int_0^t P(n,z) \sin(\omega(t-z))\, dz$$

$$= cL\alpha/n\pi \int_0^t [(-1)^n T(L,z) - T(0,z) - \bar{\theta}_c(n,z)]$$

$$\sin(n\pi c/L\,(t-z))\, dz \qquad \text{(C-14)}$$

By integrating equation C-11 by parts it is found that

$$\bar{\theta}_c(n,t) = T(L,t)(-1)^n - T(0,t) + n\pi/L \int_0^L T(x,t) \sin(n\,x/L)\, dx$$

Substituting this into equation C-14 it is seen that

$$\bar{u}_c(n,t) = -c\alpha \int_0^t \sin(n\pi c/L(t-z)) \int_0^L T(x,z) \sin(n\pi x/L)\, dx dz \qquad \text{(C-15)}$$

By using the definition of the finite Fourier transform on equation C-15 it is found that

$$u(x,t) = \frac{\bar{u}_c(0,t)}{L} -$$

$$\frac{2}{L} \sum_{n=1}^{\infty} \cos\frac{n\pi x}{L}\, c\alpha \int_0^t \sin\frac{n\pi c(t-z)}{L} dz \int_0^L T(x,z)\sin\frac{n\pi x}{L}\, dx$$

But

$$u_c(0,t) = c\alpha \int_0^t \sin(0) \int_0^L T(x,z)\, \sin(0)\, dxdz = 0$$

So

$$u(x,t) = \frac{-2c\alpha}{L} \sum_{n=1}^{\infty} \cos\left(\frac{n\pi x}{L}\right) \int_0^t \sin\left[\frac{n\pi x(t-z)}{L}\right] \int_0^L T(x,z)\sin\left(\frac{n\pi x}{L}\right) dxdz \qquad \text{(C-16)}$$

Hence, if T(x,t) is known, the stress in the bar can be obtained from equation C-2. That is

$$\sigma(x,t) = \rho c^2[\partial u(x,t)/\partial x - \alpha T(x,t)] \qquad \text{(C-17)}$$

The problem of determining T(x,t) for a two-layered wall analogous to the silicon dioxide and gold layers of the solar cell model used in the current investigation has been solved by Griffith and Horton [Ref. 40].

The solution assumed that the area of the wall was sufficiently large that the heat is conducted perpendicularly to its surface, which is taken as the plane $x = 0$. The wall consists of two components, one of thickness α, extending from the plane $x = 0$ to $x = \alpha$, while the second component extends from $x = \alpha$ to $x = \infty$.

The temperature $T(x,t)$ must satisfy the following boundary value problem

$$\partial T/\partial t = D\partial^2 T/\partial x^2 \quad t > 0,\ \alpha \geq x \geq 0;\ D = D_1 \qquad (C\text{-}18)$$

$$t > 0,\ \infty \geq x \geq \alpha;\ D = D_2$$

$$T_1(x,0) = 0 \qquad (C\text{-}19)$$

$$T_1(\alpha,t) = T_2(\alpha,t) \qquad (C\text{-}20)$$

$$k_1 \partial T_1/\partial x|_{x=\alpha} = k_2 \partial T_2/\partial x|_{x=\alpha} \qquad (C\text{-}21)$$

$$(-k_1 \partial T_1/\partial x)|_{x=0} = H \text{ for } 0 < t < \infty \qquad (C\text{-}22)$$

$$T_2(\infty,t) = 0 \text{ for } 0 < t < \infty \qquad (C\text{-}23)$$

where subscript 1 refers to the top layer 1, subscript 2 refers to the base layers 2 and

x = distance perpendicular to face of wall,

t = time,

D = thermal diffusivity = k/S,

k = thermal conductivity,

H = constant flux of heat perpendicular to the wall surface,

S = volume specific heat (specific heat times density).

The solutions to this boundary value problem are found to be:

$$T_1(x,t) = \frac{H}{k_1}\{2\sqrt{\frac{D_1 t}{\pi}}\, e^{-x^2/4D_1 t} - x(1-\mathrm{erf}\{x/2\sqrt{D_1 t}\})\}$$

$$- \frac{1}{\gamma}\sum_{n=1}^{\infty}(\frac{-1}{\gamma})^n[s\sqrt{\frac{D_1 t}{\pi}}(e^{-\{x+2\alpha(n+1)\}^2/4D_1 t} + e^{-\{x-2\alpha(n+1)^2\}/4D_1 t})$$

$$-\{x+2\alpha(n+1)\}\{1-\mathrm{erf}(\frac{x+2\alpha(n+1)}{2\sqrt{D_1 t}})\}$$

$$+\{x-2\alpha(n+1)\}\{1-\mathrm{erf}[-(\frac{x+2\alpha(n+1)}{2\sqrt{D_1 t}})]\}]\} \qquad \text{(C-23)}$$

$$T_2(x,t) = \frac{2H\lambda\sqrt{D_1}}{\gamma}\sum_{n=0}^{\infty}(\frac{-1}{\gamma})^n\{2\sqrt{\frac{D_2 t}{\pi}}\, e^{-\{x-\alpha\{1-\sqrt{D_2/D_1}(2n+1)\}\}^2/4D_2 t}$$

$$-[x-\alpha\{1-\sqrt{\frac{D_2}{D_1}}(2n+1)\}](1-\mathrm{erf}[\frac{x-\alpha\{1-\sqrt{D_2/D_1}(2n+1)\}}{2\sqrt{D_2 t}}])\} \qquad \text{(C-24)}$$

The surface temperature $T_o(t)$ is given by setting $x = 0$ in equation C-24. Then

$$T_o(t) = H/k_1 [2\sqrt{\frac{D_1 t}{\pi}} - \frac{4}{\gamma} \sum_{n=0}^{\infty} (\frac{-1}{\gamma})^n \{\sqrt{\frac{D_1 t}{\pi}} e^{-\alpha^2 (n+1)^2 / tD_1}$$

$$= \alpha(n+1)(1-\text{erf}[\frac{\alpha(n+1)}{\sqrt{D_1 t}}])\}] \qquad \text{(C-25)}$$

As can be seen, by applying equations C-24 and C-25 to equation C-17 it is, in principle, possible to predict the stress in the solar cell model as a function of both position and time. A computer code to accomplish this is available from Dr. Tom Magee of Stanford Research Institute.

APPENDIX D

NPS CO_2 Laser Operating Procedure

The following recommended procedure includes changes made to the operating procedure given by Strickland [Ref. 30] and is included as a reference for future users of the laser system. The procedure is as follows:

1. Open main valves at gas tanks and set flow rate at following values:

$He = 4.0$

$CO_2 = 5.0$

$N_2 = 4.0$

Allow a flow of four minutes before firing the laser.

2. Set trigger generator to warm-up position and allow a two-minute warm-up period. Then set trigger generator to single shot position.

3. Turn interlock switch on Circuit 8 to the "ON" position. This activates the red warning lights at entrances to the laboratory and puts power to the DC power supply of the laser.

4. Ensure that the north door to the laboratory is locked to prevent unwary individuals from entering by this means.

5. Turn on DC power supply utilizing the switch located on front cover. This will light both the amber and green lights on the power supply. Allow a two-minute warm-up period.

6. Put on safety goggles with plexiglass window.

7. Set Marx generator spark gap pressure corresponding to desired firing voltage following posted chart.

8. Set desired Marx generator discharge voltage on variac at the DC power supply.

9. Set Marx generator charging voltage on preset voltage meter at the DC power supply. The voltage set should be one-third of the Marx discharge voltage.

10. Initiate charging of the system by pressing the remote charge switch mounted next to the trigger generator or by pressing the "CHARGE" switch at the DC power supply. This will extinguish the green light and activate the red light on the power supply.

11. When the preset voltage level is reached, the audible alarm will be activated and the red light will be extinguished. Firing of the laser can now be accomplished by pushing the button on the trigger generator. If the laser is not fired within five seconds after completion of charging the automatic dump operates and the system is discharged to ground.

12. If necessary, the system can be dumped at any time after initiation of charging either with the remote dump switch at the trigger generator or the local dump switch at the DC power supply.

13. Further firing at the preset voltage can be accomplished by repeating the procedure beginning at step 8 or at another voltage beginning at step 5.

APPENDIX E

NPS CO_2 Laser Alignment Procedure

The following alignment procedure is suggested for future users of the CO_2 Laser System. It should be implemented whenever the output of the laser is found to have significantly changed or when the Sodium Chloride (NaCl) Brewster windows are installed after polishing. The alignment procedure requires, in addition to the CO_2 laser itself, the following equipment:

1. Helium-Neon (HeNe) CW laser with laser aligner attachment.
2. CO_2 laser alignment blocks (2)
3. HADRON Ballistic Thermopile
4. Millimicrovoltmeter
5. Copper Mirror (f = 1.0 m).

The alignment procedure assumes that the NaCl windows are not installed at initiation of the procedure. It is broken into two sections: rough alignment and fine tuning. Referring to Figure 25, the procedure is as follows:

A. Rough Alignment

1. Remove Germanium exit mirror and its mount.
2. Install laser alignment blocks.
3. Install NaCl windows.
4. Mount HeNe laser about 1.0 meter in front of output end of CO_2 laser.

5. Adjust beam from HeNe laser so that it passes through the holes in center of laser alignment blocks.

6. Place a sheet of Mylar between output end of CO_2 laser and HeNe laser.

7. Adjust Copper Mirror (f = 3.0 m) at back end of CO_2 laser resonant cavity until the beam from the HeNe laser reflected by this mirror passes back through holes in alignment blocks onto the Mylar sheet.

8. Adjust the Copper Mirror until the reflected beam is coincident with the beam from the HeNe laser incident on the Mylar.

9. Reinstall Germanium output mirror and mount.

10. Adjust germanium mirror until the HeNe beam reflected from this window onto the Mylar sheet is coincident with the incident beam.

11. The CO_2 laser is now rough aligned. Remove the laser alignment blocks. This will require removal of the NaCl windows. When removing these windows do not change their orientation.

12. Reinstall NaCl windows.

13. Remove HeNe laser and Mylar sheet.

14. Place a sheet of laser "footprint" paper about 20 cm in front of the germanium output window.

15. Light off the CO_2 laser system.

16. Starting at about 30 kV discharge voltage from Marx generator fire the laser. If no beam footprint is observed

on the footprint paper, increase the discharge voltage in increments of 3 kV until a footprint is seen. Do not exceed 45 kV at this stage of alignment. When footprint of laser beam is seen proceed to step 17.

17. Remove footprint paper and begin fine tuning the laser.

B. Fine Tuning

18. Install 1.0 meter focal length copper mirror about 1.0 meter from output window of laser.

19. Connect input lead of voltmeter to calibration terminals of ballistic thermopile.

20. Mount ballistic thermopile about 1.0 m from copper mirror of step 18.

21. Adjust copper mirror so that beam from CO_2 laser enters INPUT cone of ballistic thermopile.

22. Using the voltmeter to monitor the total laser energy output adjust the mirror at back end of laser resonant cavity until laser energy output is at a maximum. A wait of about two minutes between laser firings will yield best results.

23. Repeat step 22 with germanium output mirror of CO_2 laser. This completes the alignment procedure. A calibration curve for laser output as a function of discharge voltage may now be obtained.

APPENDIX F

COMPUTER CODE TO CALCULATE PEAK PRESSURE PULSES

THIS PROGRAM IS DESIGNED TO CALCULATE PEAK PRESSURE PULSES GENERATED IN A GALLIUM ARSENIDE SOLAR CELL MODEL AS THE SILICON DIOXIDE AND GOLD LAYERS ARE SUCCESSIVELY REMOVED IN 50 ANGSTROM DECREMENTS. THE CODE FIRST CALCULATES THE REFLECTANCE AND ABSORPTANCE OF THE MODEL FOLLOWING THE METHOD GIVEN BY HEAVENS (REF.36). THE ABSORPTANCE SO-CALCULATED IS THEN APPLIED TO THE LASER ENERGY OUTPUT (EN, EN1) TO GET THE ENERGY DENSITY INCIDENT ON THE TARGET (ED, ED1). THE VALUE OF ENERGY DENSITY IS THEN APPLIED TO GET THE PRESSURE GENERATED IN BOTH ATMOSPHERIC AND VACUUM PRESSURE CONDITIONS.

THE VARIOUS LAYERS OF THE SOLAR CELL MODEL ARE IDENTIFIED BY A NUMERICAL DESIGNATION AS FOLLOWS:

1. AIR
2. SILICON DIOXIDE
3. GOLD
4. GALLIUM ARSENIDE
5. QUARTZ GAUGE (SILICON DIOXIDE).

THE INITIAL THICKNESS (D) AND THE REAL AND IMAGINARY PARTS OF THE INDEX OF REFRACTION (RR AND RI) FOR EACH LAYER ARE READ IN WITH A MATRIX NOTATION. ANOTHER MATRIX IS USED TO ENTER THE VALUES OF DENSITY (RHO) AND SOUND SPEED (V) FOR EACH MATERIAL. TWO MATRICES ARE USED SINCE THE VALUES OF RR AND RI ARE WAVELENGTH DEPENDENT AND CAN THUS BE CHANGED WITHOUT AFFECTING THE VALUES OF RHO AND V.

THE COMPUTER PROGRAM FOLLOWS.

```
ENTER JCECARDS.
      //CLICKRUN
       JFJ001 FORTGO (2720,0420,WS44),'JACOBSONSMC1499'

DIMENSION MATRICES USED.
      DIMENSION RR(5),RI(5),D(5),RHO(5),V(5)

ENTER VALUE OF WAVELENGTH IN METERS. (WA).
      WA=10.6E-06
ENTER LASER SPOT RADIUS IN METERS (RA).
      RA=6.5E-03

ENTER PULSE LENGTH (TP) AND PRESSURE PULSE DURATION AT
ATMOSPHERIC PRESSURE (T). BOTH OF THESE QUANTITIES ARE IN
UNITS OF SECONDS.
      TP=250.0E-09
      T=5.0E-07

ENTER LASER ENERGY OUTPUT (ENL) IN JOULES.
      ENL=5.25

READ IN AND PRINT OUT THE VALUES OF D(I), RR(I), AND RI(I).
D(I) IS IN UNITS OF METERS.
      PI=3.14159
      READ (5,500) (RR(I),RI(I),D(I),I=1,5)
  500 FORMAT (3E10.3)
      WRITE (6,600) (RR(I),RI(I),D(I),I=1,5)
  600 FORMAT (//,10X,3E10.3)
      WRITE (6,601)
  601 FORMAT (//)
READ IN AND PRINT OUT THE DENSITY AND VELOCITY MATRICES.
      READ (5,501) (RHO(J),V(J),J=2,5)
  501 FORMAT (2E10.3)
      WRITE (6,604) (RHO(K),V(K),K=2,5)
  604 FORMAT (//,5X,2E10.2)
      WRITE (6,601)
CALCULATE AND PRINT OUT THE ACOUSTIC IMPEDANCES FOR USE IN
CALCULATING THE PRESSURE IN VACUUM.
      Z2=RHO(2)*V(2)
      Z3=RHO(3)*V(3)
      Z4=RHO(4)*V(4)
```

```
      WRITE (6,610) Z2,Z3,Z4
  610 FORMAT (10X,3E10.3)
      WRITE (6,601)

CALCULATE THE ENERGY DENSITIES IN JOULES PER SQUARE METER.
THE ENERGY DENSITY ED INCLUDES THE CORRECTION FOR THE
GERMANIUM ENTRANCE WINDOW AND IS USED FOR VACUUM PRESSURES.
ED1 ONLY CORRECTS FOR THE GERMANIUM LENS AND IS USED FOR
ATMOSPHERIC PRESSURE CALCULATIONS.
      EN=0.693*ENL
      EN1=0.9*ENL
      ED=EN/((PI)*(RA**2))
      ED1=EN1/((PI)*(RA**2))
      WRITE (6,615) ED1
      WRITE (6,601)
      WRITE (6,608) ED
  608 FORMAT (5X,'ENERGY DENSITY IS',1E10.3)
  615 FORMAT (5X,'ATMOSPHERE ENERGY IS',1E10.3)
      WRITE (6,601)
AT THIS POINT THE REFLECTANCE OF THE SYSTEM OF THIN FILMS
IS BEGUN TO BE CALCULATED. FIRST THE TERMS INDEPENDENT OF
FILM THICKNESS ARE CALCULATED AND PRINTED.
      A2=(RR(1)**2)+(RI(1)**2)-(RR(2)**2)-(RI(2)**2)
      B2=((RR(1)+RR(2))**2)+((RI(1)+RI(2))**2)
      C2=2.0*((RR(1)*RI(2))-(RR(2)*RI(1)))
      A3=(RR(2)**2)+(RI(2)**2)-(RR(3)**2)-(RI(3)**2)
      B3=((RR(2)+RR(3))**2)+((RI(2)+RI(3))**2)
      C3=2.0*((RR(2)*RI(3))-(RR(3)*RI(2)))
      A4=(RR(3)**2)+(RI(3)**2)-(RR(4)**2)-(RI(4)**2)
      B4=((RR(3)+RR(4))**2)+((RR(3)+RI(4))**2)
      C4=2.0*((RR(3)*RI(4))-(RR(4)*RI(3)))
      G2=A2/B2
      G3=A3/B3
      G4=A4/B4
      H2=C2/B2
      H3=C3/B3
      H4=C4/B4
      WRITE (6,606)
  606 FORMAT (14X,'G1',9X,'G2',9X,'G3',9X,'G4')
      WRITE (6,605) G1,G2,G3,G4
  605 FORMAT (10X,4E10.3)
      WRITE (6,601)
      WRITE (6,607)
  607 FORMAT (14X,'H1',9X,'H2',9X,'H3',9X,'H4')
      WRITE (6,605) H1,H2,H3,H4
      WRITE (6,601)

THE RADIAL WAVELENGTH IS NOW CALCULATED.
      W=(2.0*PI)/WA

AT THIS POINT THE TERMS OF THE REFLECTANCE DEPENDENT UPON
THE THICKNESSES OF THE FILMS ARE CALCULATED AND THE PRESSURE
FOR THE VACUUM AND ATMOSPHERIC CASES ARE THEN COMPUTED.
THIS IS DONE BY THE USE OF TWO DO LOOPS. THE FIRST STARTS
WITH THE INITIAL THICKNESS OF THE SILICON DIOXIDE LAYER AND
REMOVES IT IN 50 ANGSTROM DECREMENTS. WHEN THIS LAYER HAS
BEEN TOTALLY REMOVED THE CODE SHIFTS TO THE SECOND DO LOOP
AND REPEATS THE PROCEDURE FOR THE GOLD LAYER.

CALCULATE THE TERMS OF THE REFLECTANCE OF THE SILICON
DIOXIDE/GOLD SYSTEM THAT ARE THICKNESS DEPENDENT.
      DO 15 K=1,50
      ALF2=W*D(2)*RI(2)
      GAM2=W*D(2)*RR(2)
      E2=EXP(ALF2)
      D2=COS(GAM2)
      D3=SIN(GAM2)
      P3=E2*D2
      Q3=E2*D3
      T3=((G3*D2)+(H3*D3))/E2
      L3=((H3*D2)-(G3*D3))/E2
CALCULATE THE REFLECTANCE, R, OF THE SYSTEM.
```

```
      P23=P3+(G2*T3)-(H2*U3)
      Q23=Q3+(H2*T3)+(G2*U3)
      T23=T3+(G2*P3)-(H2*Q3)
      U23=U3+(H2*P3)+(G2*Q3)
      R=((T23**2)+(U23**2))/((P23**2)+(Q23**2))
CALCULATE THE ABSORPTANCE OF THE SYSTEM, A.
      A=1.0-R
CACLLATE THE PRESSURE GENERATED IN THE GOLD LAYER OF THE
SOLAR CELL MODEL FOR THE VACUUM (PBAR) AND THE ATMOSPHERIC
(PPBAR) CASES. UNITS ARE IN BARS.
      PR2=Z3*A*ED/(3.0*TP)
      PP=SQRT(PR2)
      PBAR=PR/1.0E05
      PP=(A*ED1)/(V(3)*T)
      PPBAR=PP/1.0E05
CORRECT THESE PRESSURES FOR THE VALUES EXPECTED IN THE
GALLIUM ARSENIDE LAYER (PGAAS AND PPGAAS RESPECTIVELY.).
      PGAAS=0.43*PBAR
      PPGAAS=0.43*PPBAR
PRINT THE VALLES OF R, A, PBAR, PGAAS,PPBAR, AND PPGAAS
CORRESPONDING TO LAYER THICKNESS D(2).
      WRITE (6,602) D(2),R,A,PBAR,PGAAS,PPBAR,PPGAAS
  602 FORMAT (5X,7E12.4)
REDUCE THE THICKNESS OF THE SILICON DIOXIDE LAYER BY 50
ANGSTROMS AND DETERMINE IF IT HAS BEEN COMPLETELY REMOVED.
IF IT HAS SHIFT TO THE NEXT DO LOOP. IF NOT REPEAT ABOVE
COMPUTATIONS FOR THE NEW VALUE OF D(2).
      D(2)=D(2)-5.0E-09
      IF (D(2).LE.0.00) GO TO 21
   15 CONTINUE

   21 DO 22 L=1,50
      ALF3=W*D(3)*RI(3)
      GAM3=W*D(3)*RR(3)
      DC3=COS(GAM3)
      DS3=SIN(GAM3)
      E3=EXP(ALF3)
      P4=E3*DC3
      Q4=E3*DS3
      T4=((G4*DC3)+(H4*DS3))/E3
      U4=((H4*DC3)-(G4*DS3))/E3
      P34=P4+(G3*T4)-(H3*U4)
      Q34=Q4+(H3*T4)+(G3*U4)
      T34=T4+(G3*P4)-(H3*Q4)
      U34=U4+(H3*P4)+(G3*Q4)
COMPUTE THE REFLECTANCE OF THIS NEW SYSTEM WHEREIN THE
SILICON DIOXIDE LAYER HAS BEEN ENTIRELY REMOVED.
      RP=((T34**2)+(U34**2))/((P34**2)+(Q34**2))
CALCULATE THE ABSORPTANCE OF THE SYSTEM, AP.
      AP=1.0-RP
CALCULATE THE VACUUM (PRBAR) AND ATMOSPHERE (RBAR)
PRESSURES, CORRECT THEM TO THE VALUES EXPECTED IN THE
GALLIUM ARSENIDE LAYER (PG AND PPGR) AND PRINT THE VALUES
OF RP, AP, PBAR, PG, RBAR, AND PPGR FOR CORRESPONDING
THICKNESS OF THE GOLD LAYER D(3).
      PR2P=Z4*AP*ED/(3.0*TP)
      PRP=SQRT(PR2P)
      PRBAR=PRP/1.0E05
      PG=0.43*PRBAR
      PPR=(ED1*AP)/(V(4)*T)
      RBAR=PPR/1.0E05
      PPGR=0.43*RBAR
      WRITE (6,602) D(3),RP,AP,PRBAR,PG,RBAR,PPGR
DECREMENT THE GOLD LAYER BY 50 ANGSTROMS AND REPEAT THE
CALCULATIONS. IF LAYER HAS BEEN COMPLETELY REMOVED
TERMINATE THE PROGRAM.
      D(3)=D(3)-5.0E-09
      IF (D(3).LE.0.00) GO TO 20
   22 CONTINUE
   20 STOP
      END
$ DATA
```

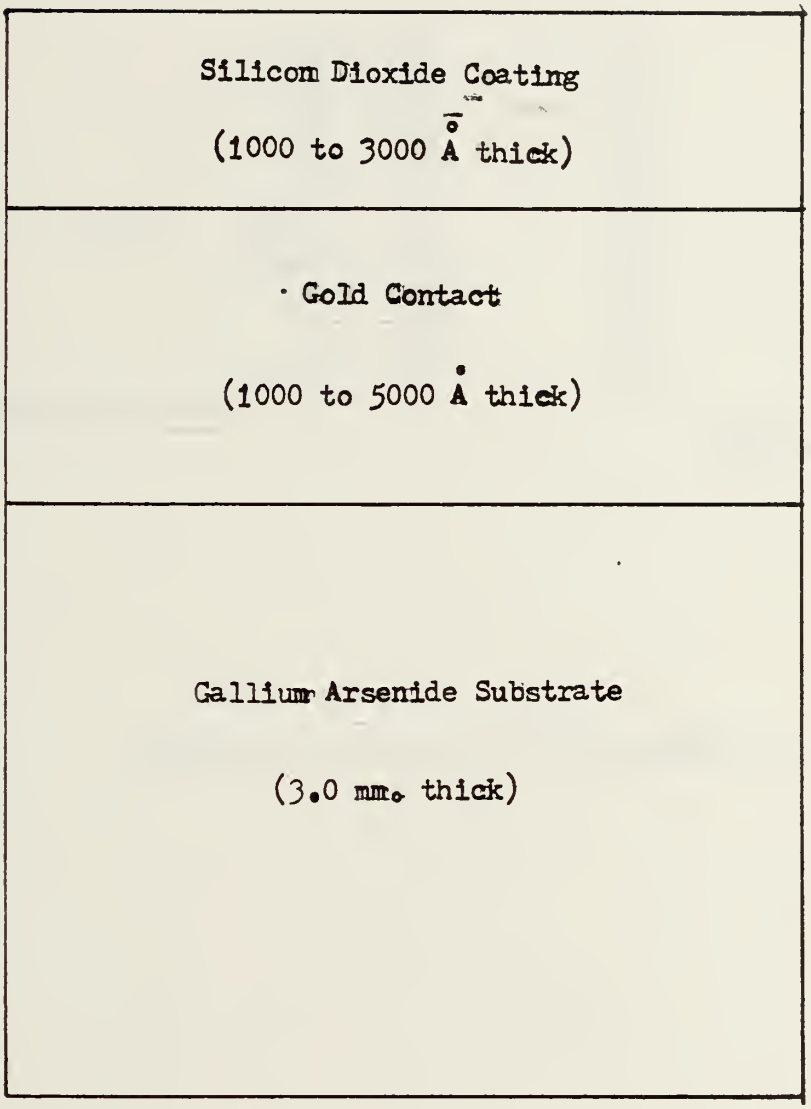

GaAs Solar Cell Model

Figure 1

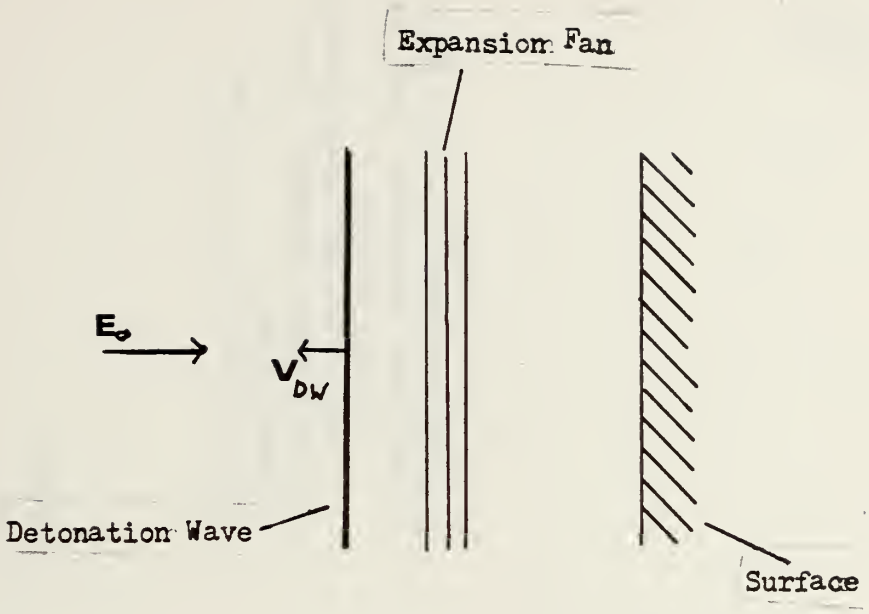

Detonation Wave Model for One Dimension

Figure 2

Diagram of Experimental Arrangement

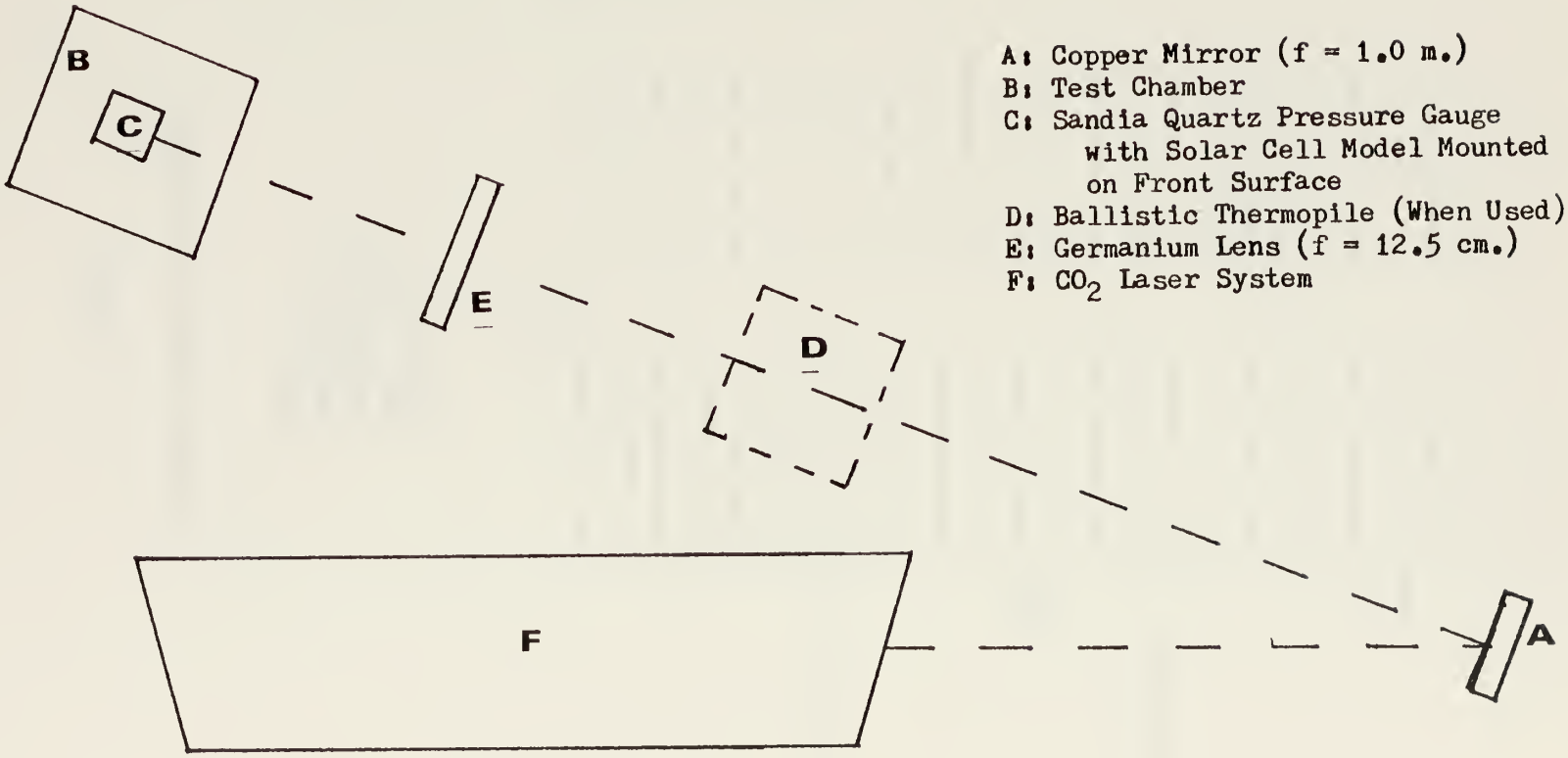

A: Copper Mirror (f = 1.0 m.)
B: Test Chamber
C: Sandia Quartz Pressure Gauge with Solar Cell Model Mounted on Front Surface
D: Ballistic Thermopile (When Used)
E: Germanium Lens (f = 12.5 cm.)
F: CO_2 Laser System

Figure 3

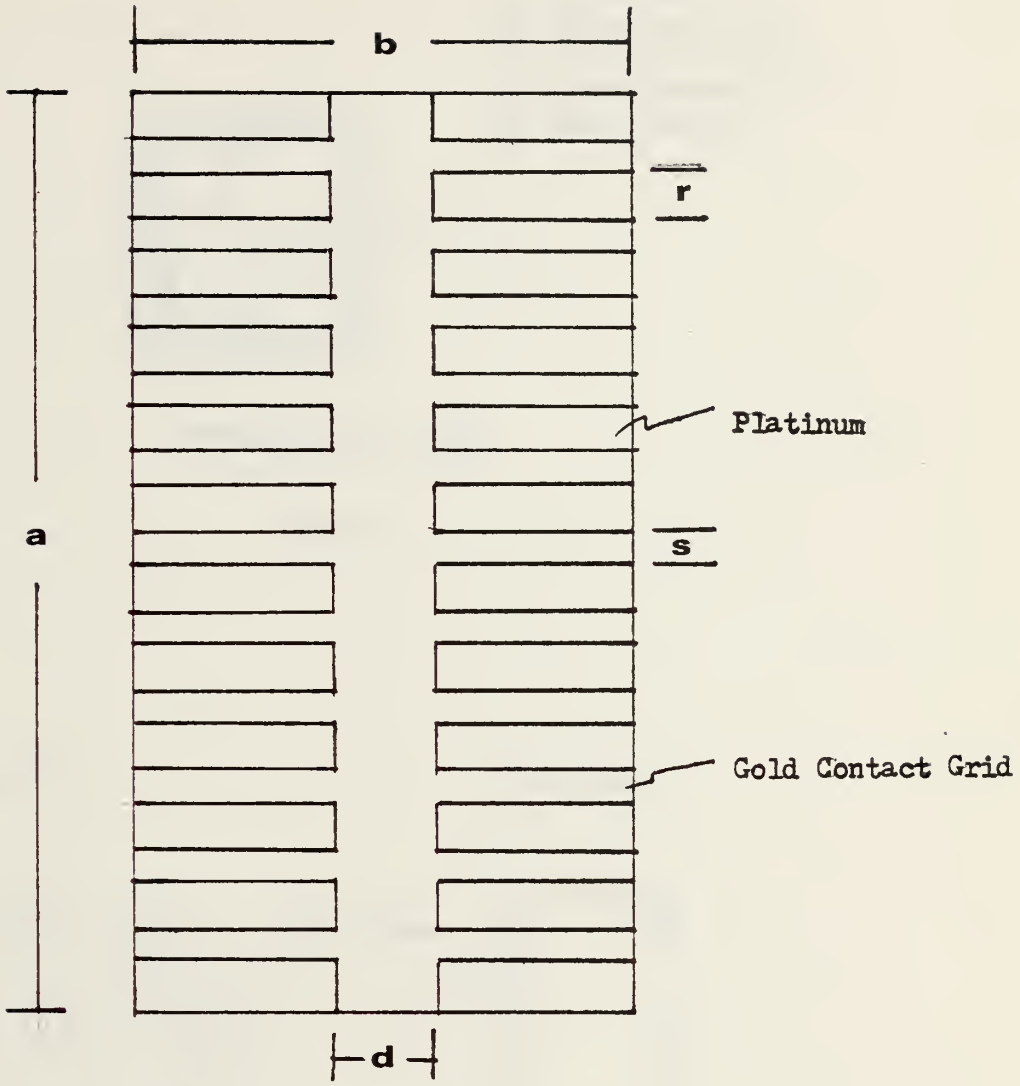

a = 1.25 cm.
b = 1.0 cm.
d = 0.08 cm.
r = 0.05 cm.
s = 0.005 cm.

Gridded Solar Cell Geometry

Figure 4

A: X-cut Quartz
B: Solar Cell Model
C: Microcoaxial Cable
D: Aluminum Housing
E: Epoxy Cement

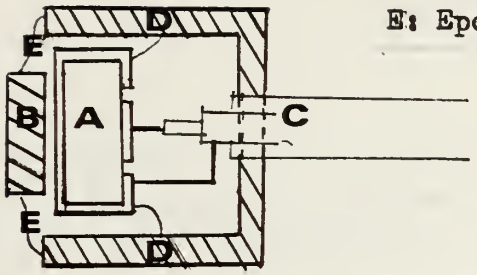

Sandia Quartz Gauge

Figure 5

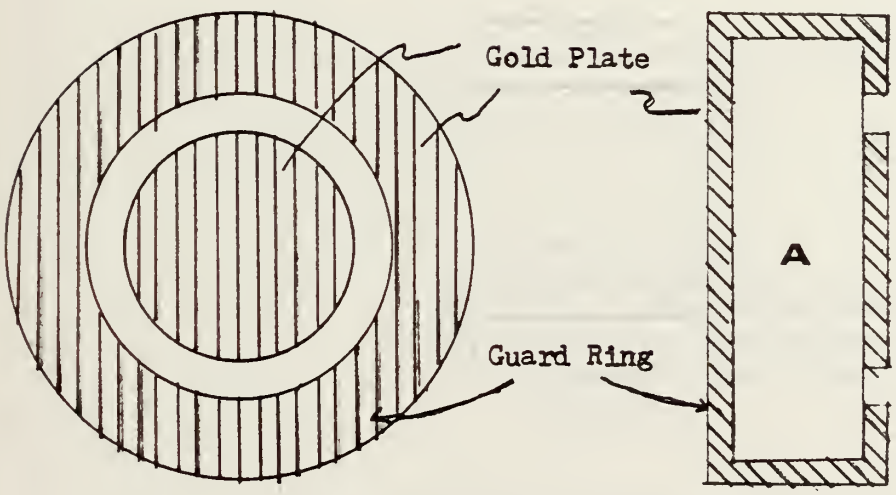

Guard Ring Configuration

Figure 6

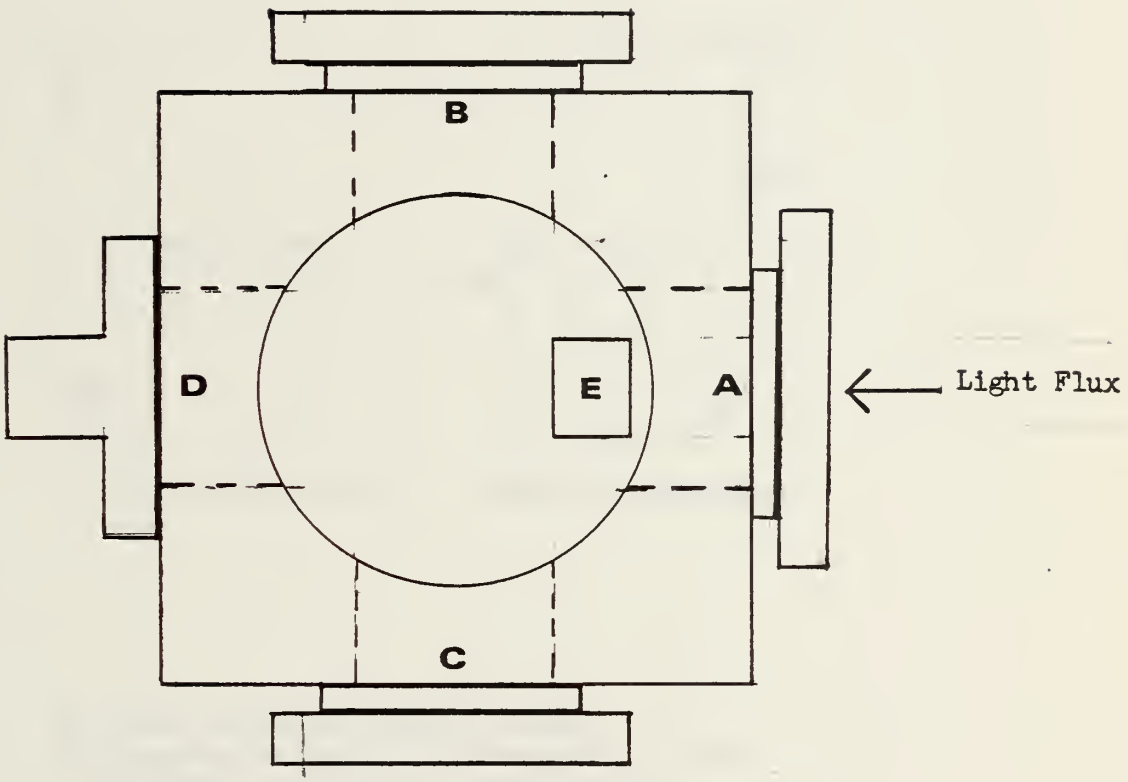

A: Entrance Window
B, C: Quartz Windows
D: Vacuum System Connection
E: Position of Quartz Gauge with Solar Cell Model Attached

Diagram of Overhead View of Test Chamber

Figure 7

Marx Generator of CO_2 Laser

Quartz Gauge

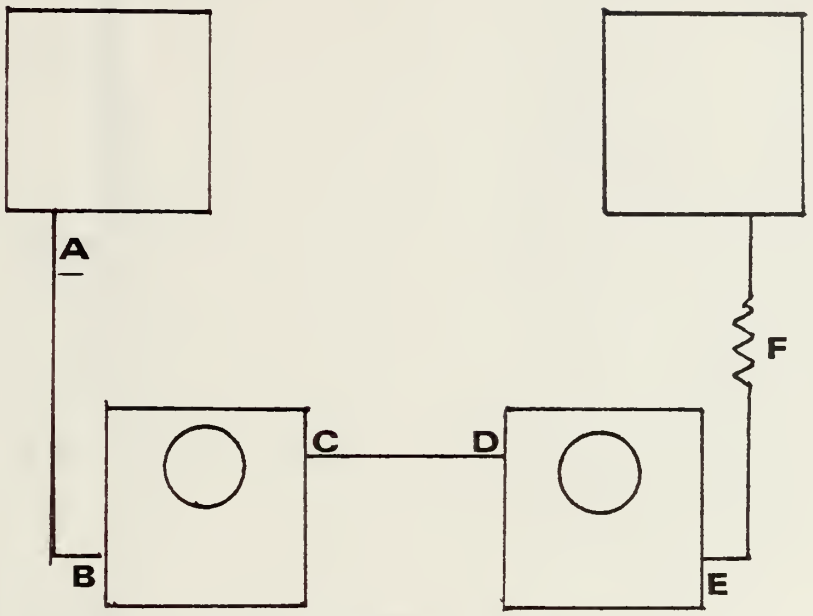

T-555 Oscilloscope

T-7704 Oscilloscope

A: Marx Generator Current Output
B: External Trigger In Connection of T-555
C: External Trigger Out Connection of T-555 with 1.0 μsec. Delay
D: External Trigger In Connection of T-7704
E: External Input Connection of T-7704
F: 50 Ohm Termination

Experimental Circuitry

Figure 8

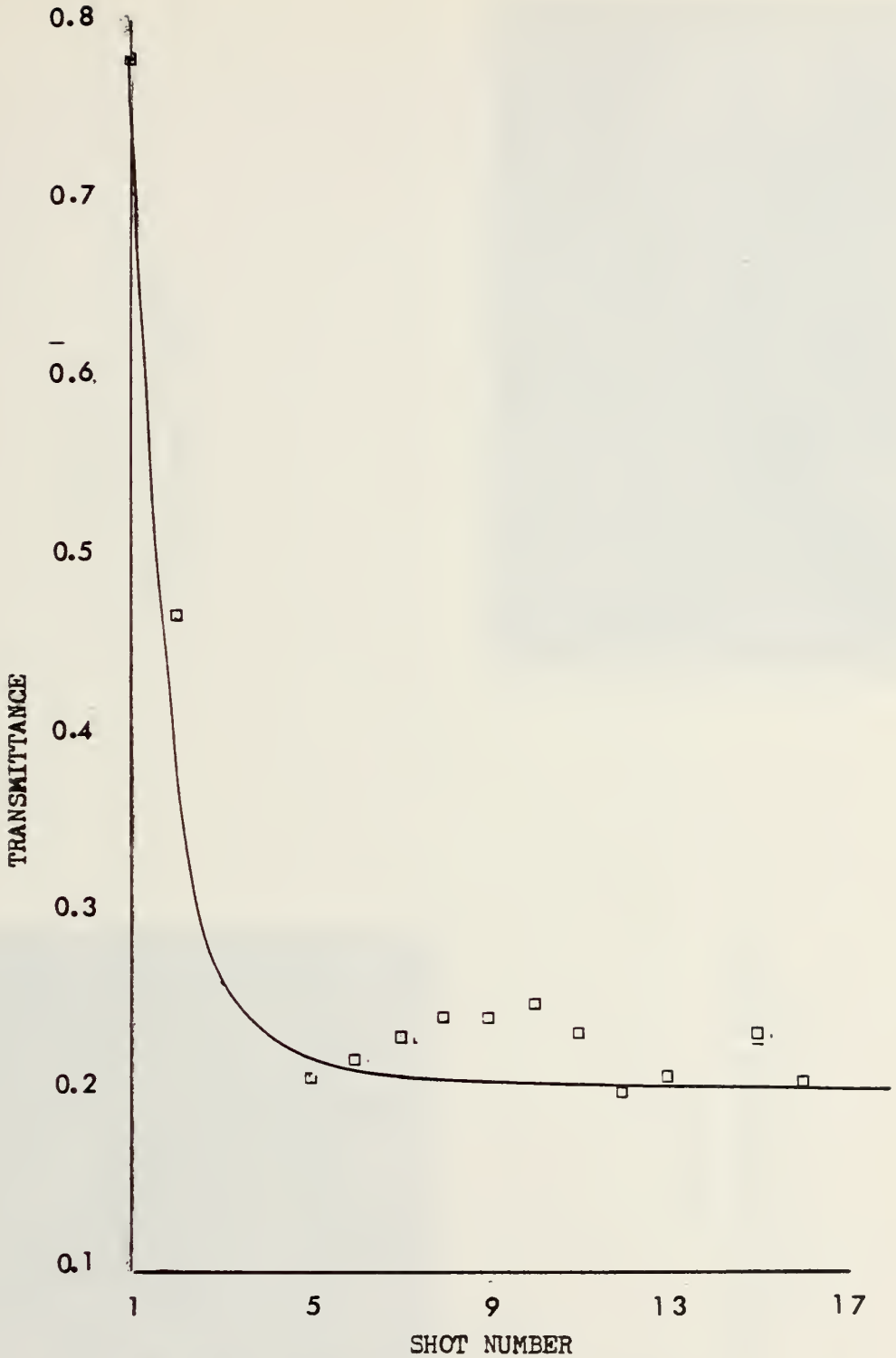

Transmittance Curve for Germanium Window

Figure 9

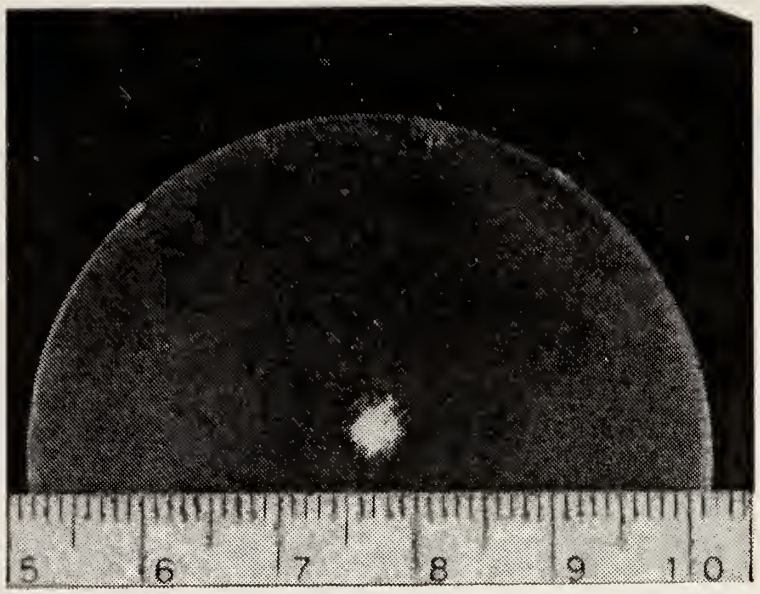

Figure 10

Damage to NaCl Window
after Three Shots

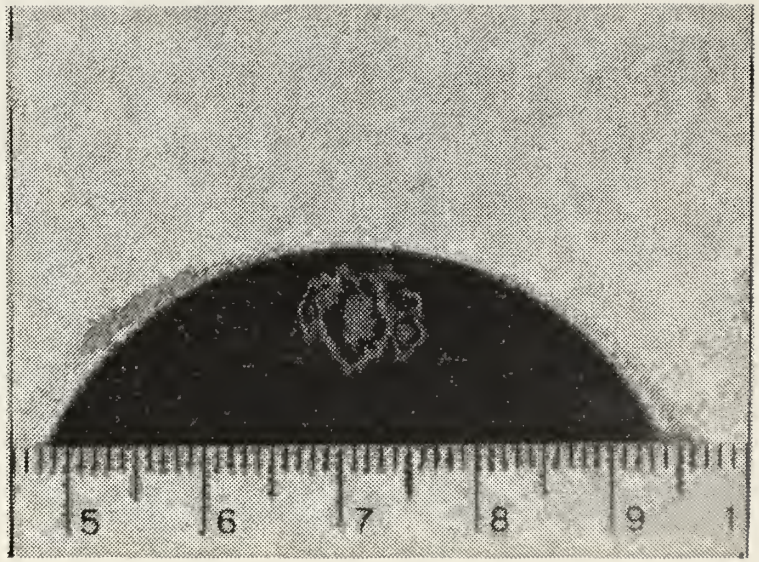

Figure 11

Damage to Germanium Window
after Sixteen Shots

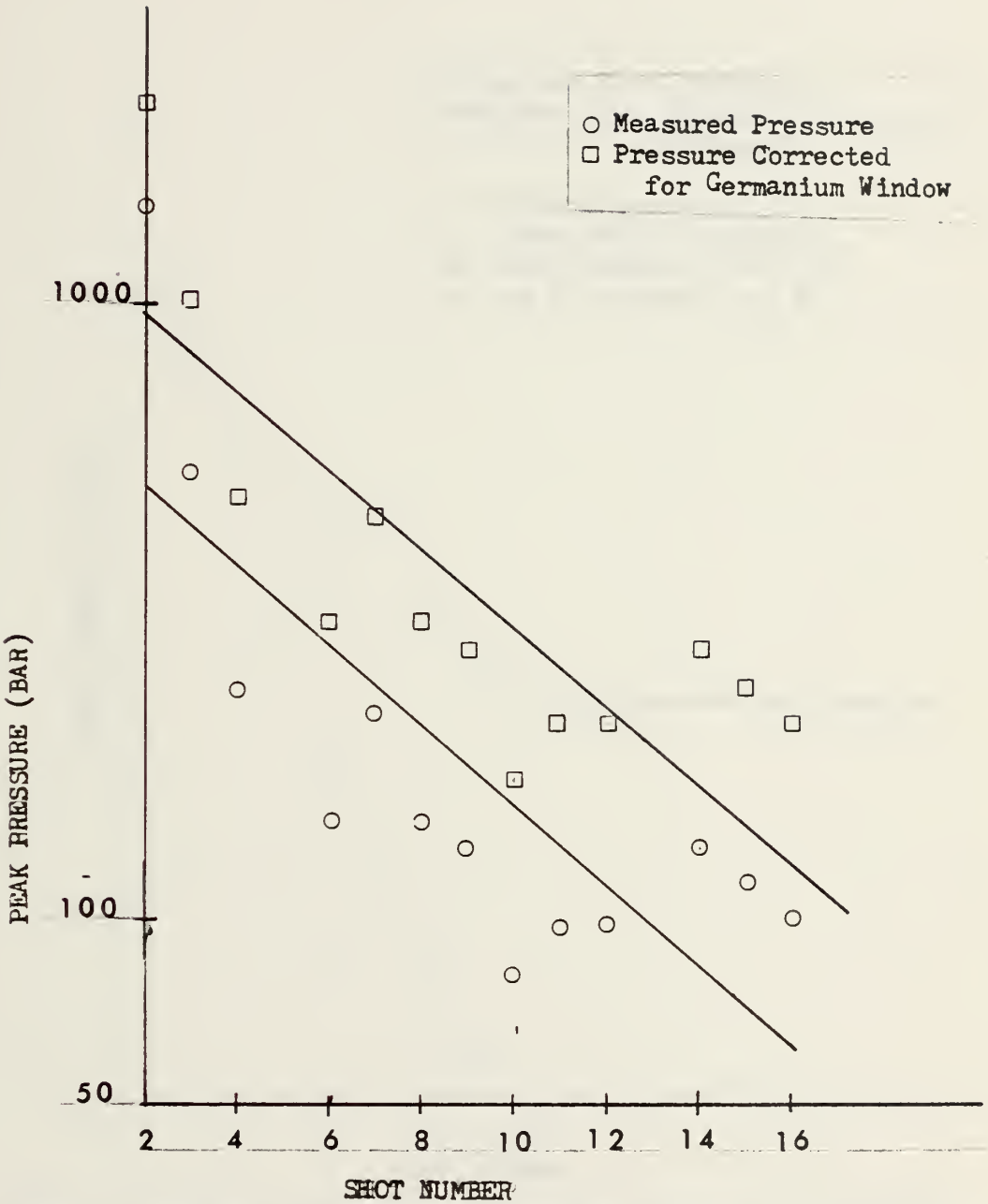

Graph of Peak Pressure versus Shot Number for 1000/1000 System in Vacuum

Figure 12

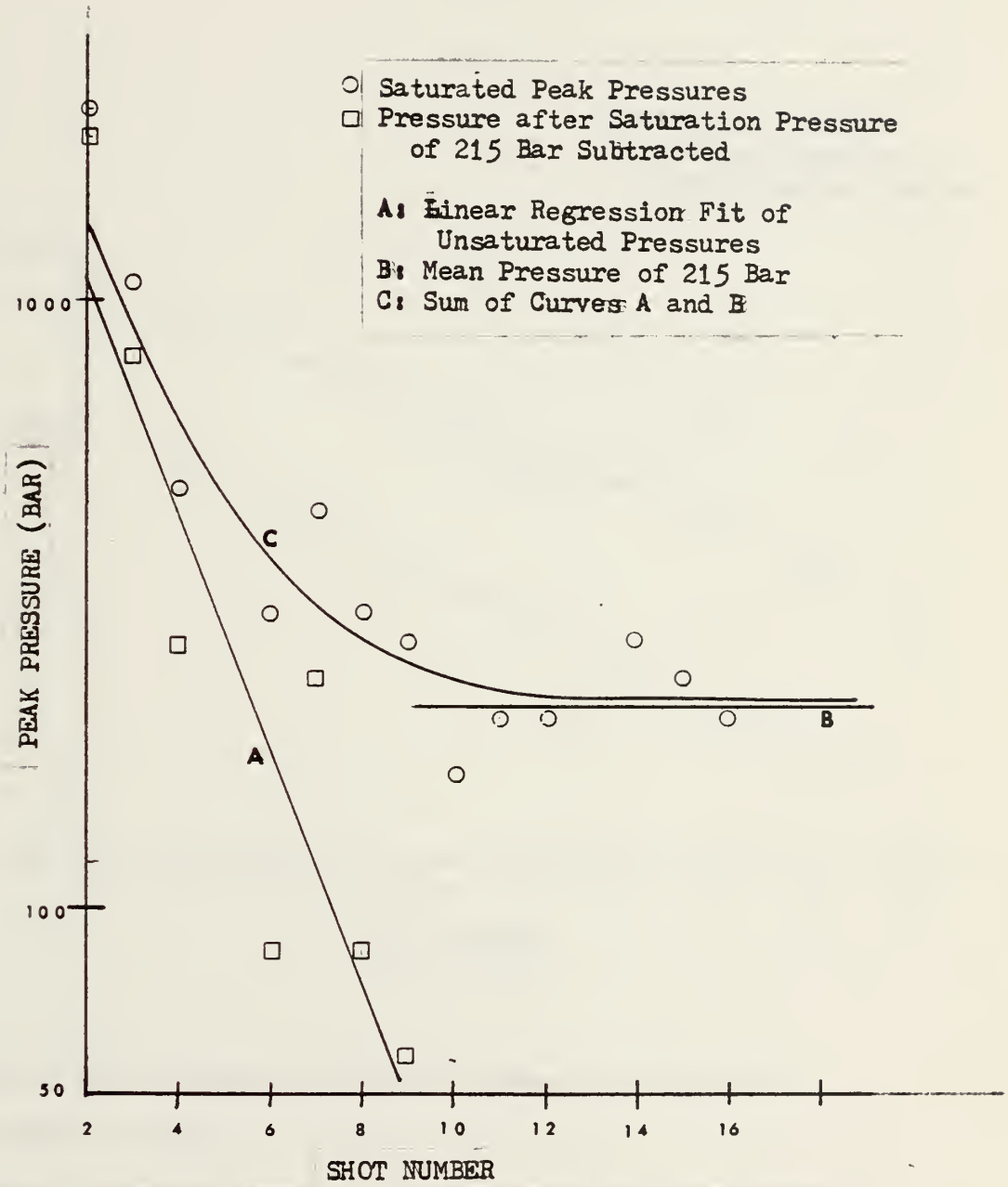

Graph of Unsaturated Pressure Versus Shot Number for 1000/1000 System in Vacuum

Figure 13

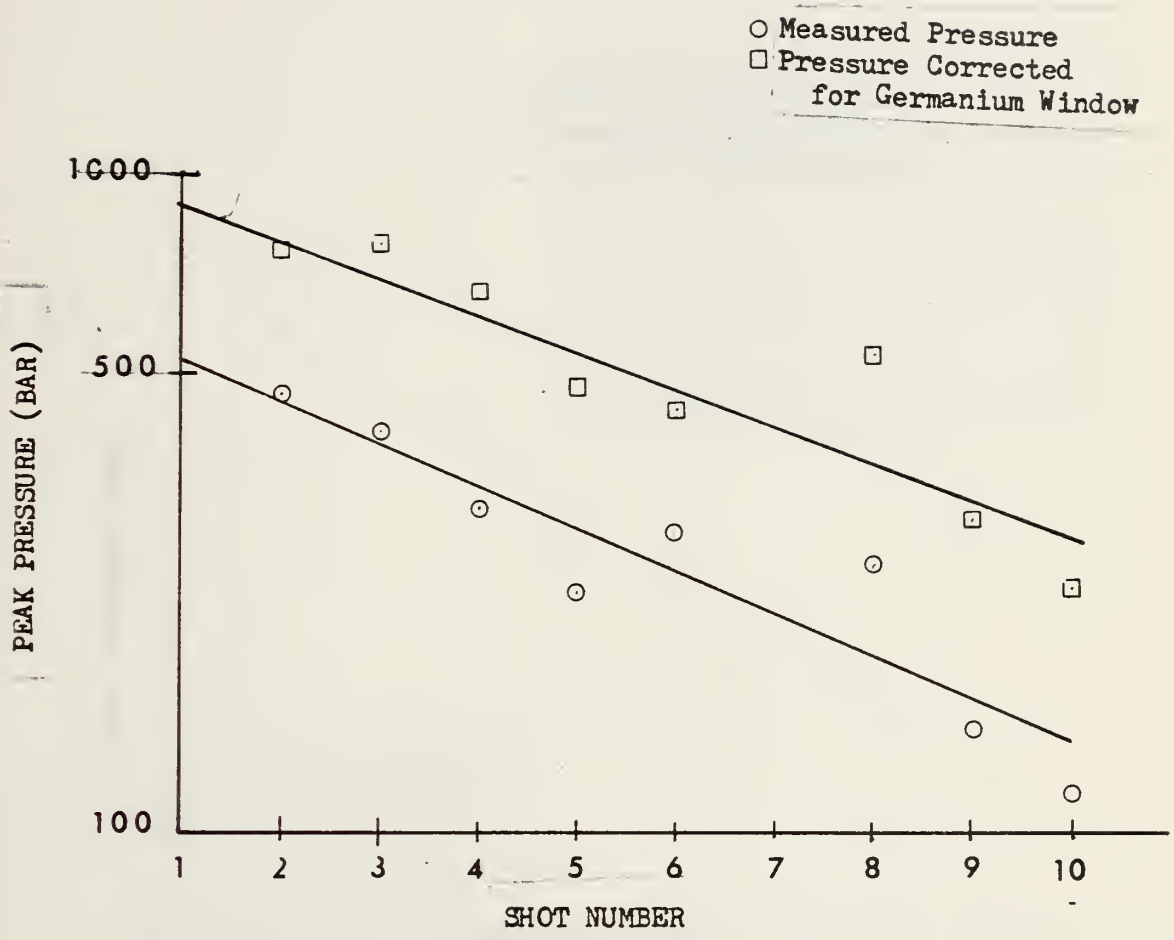

Graph of Peak Pressure Versus Shot Number for 1000/2000 System in Vacuum

Figure 14

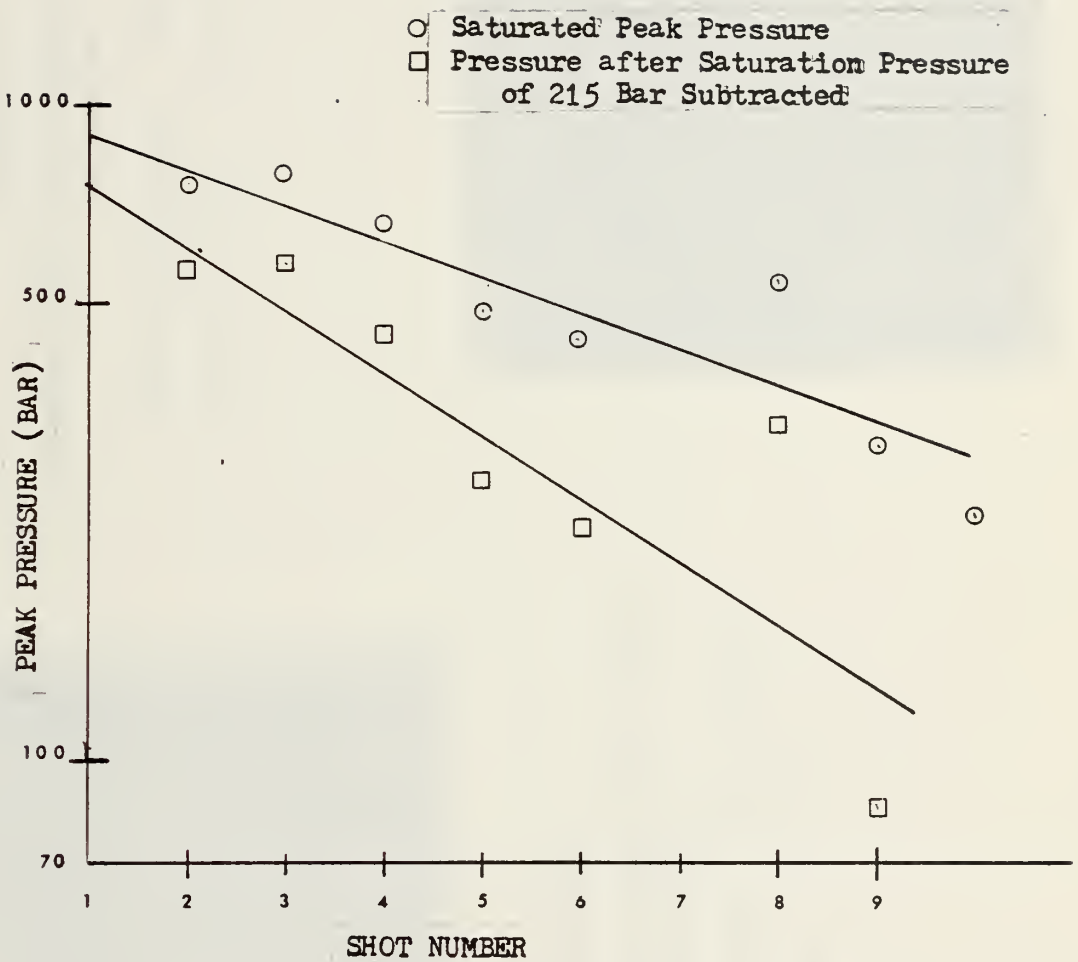

Graph of Unsaturated Pressure Versus Shot Number for 1000/2000 System in Vacuum

Figure 15

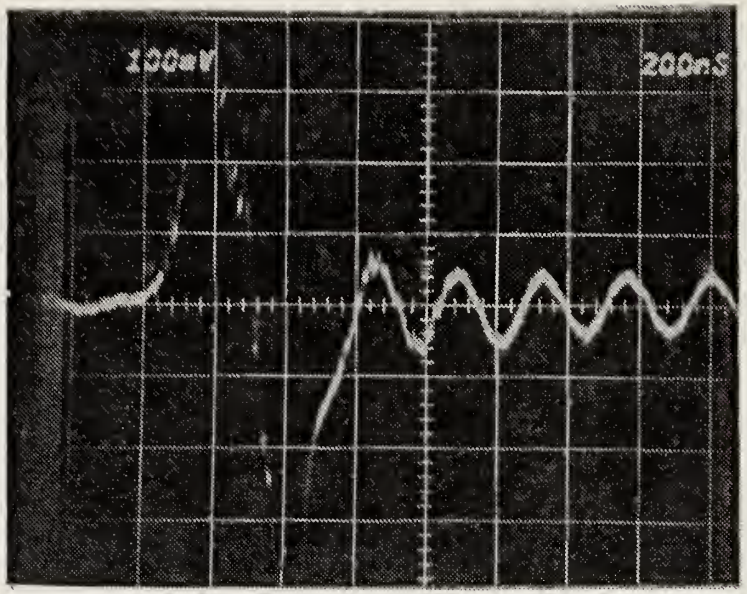

Figure 16

Early Pulse for 1000/1000 System in Vacuum

Horizontal Scale: 200 nsec/cm

Vertical Scale: 100 mV/cm

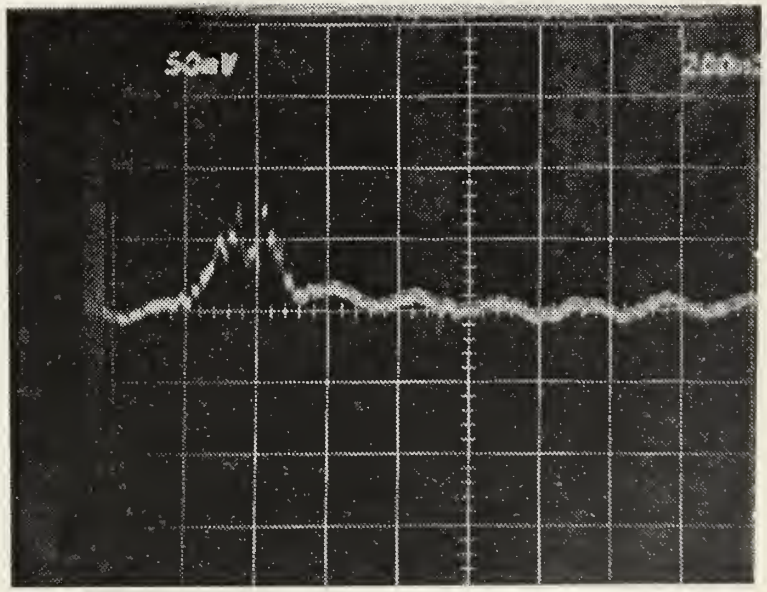

Figure 17

Final Pulse for 1000/1000 System in Vacuum

Horizontal Scale: 200 nsec/cm

Vertical Scale: 50 mV/cm

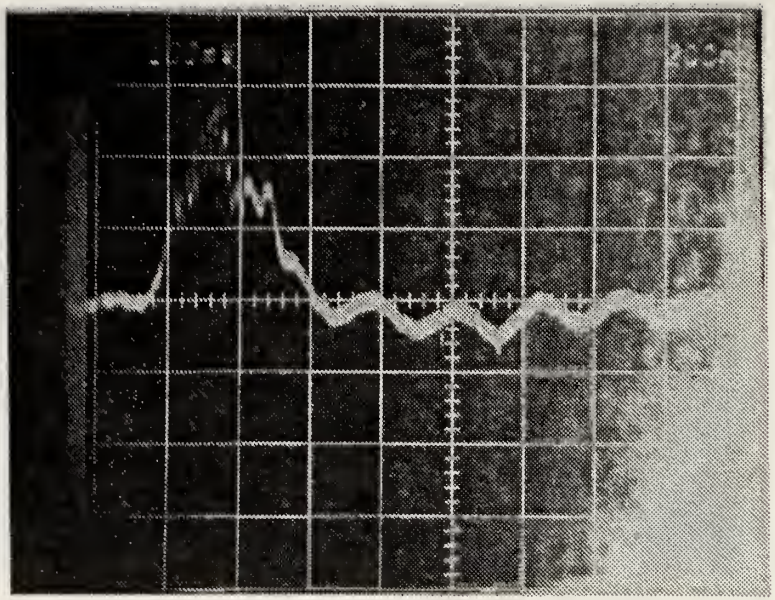

Figure 18

Early Pulse for 1000/2000 System in Vacuum

Horizontal Scale: 200 nsec/cm

Vertical Scale: 100 mV/cm

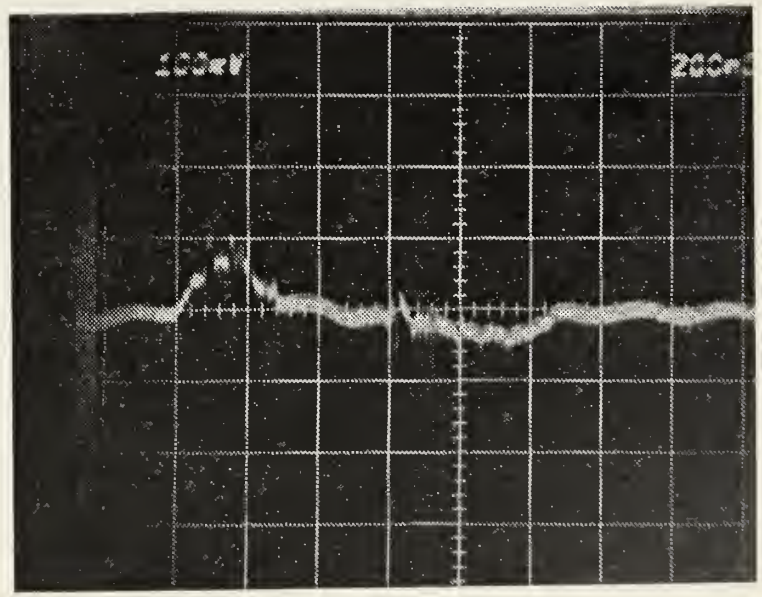

Figure 19

Final Pulse for 1000/2000 System in Vacuum

Horizontal Scale: 200 nsec/cm

Vertical Scale: 100 mV/cm

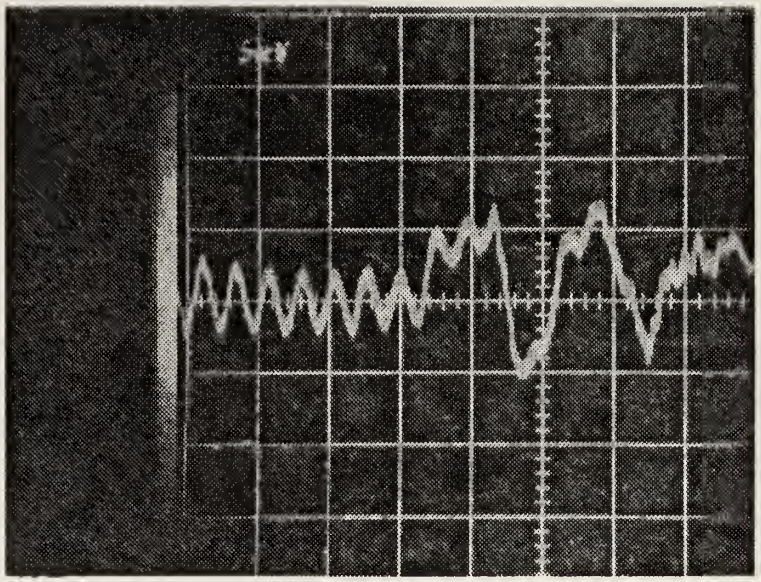

Figure 20

Typical Pulse for 1000/2000 System
at Atmospheric Pressure

Horizontal Scale: 500 nsec/cm

Vertical Scale: 5 mV/cm

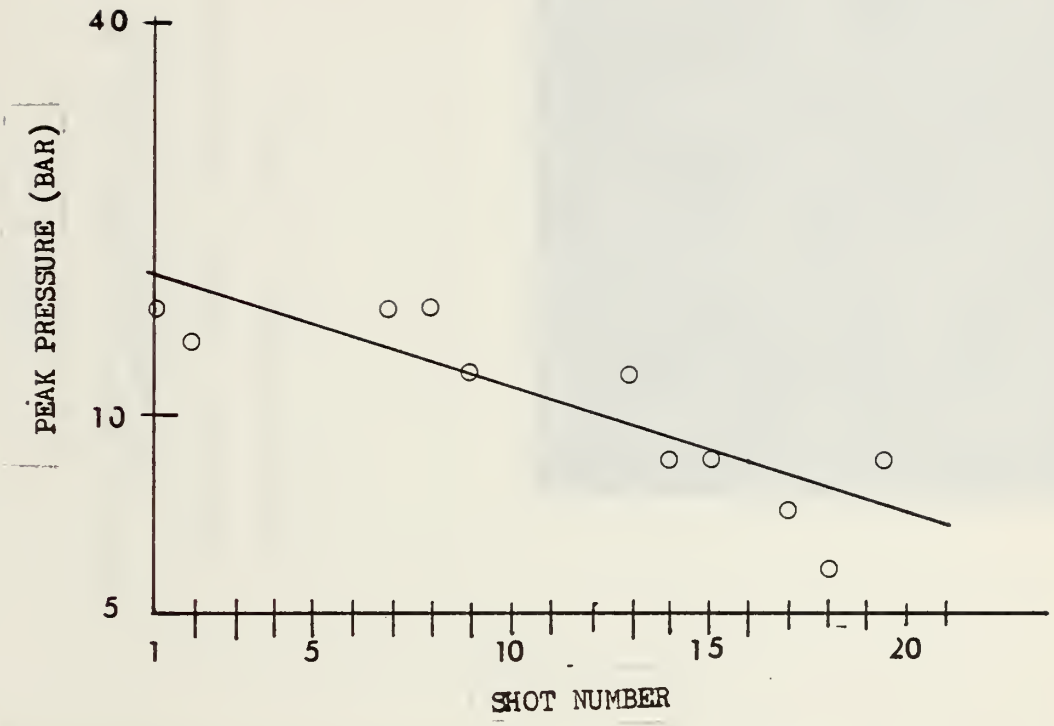

Graph of Peak Pressure Versus Shot Number for 1000/2000 System at Atmospheric Pressure

Figure 21

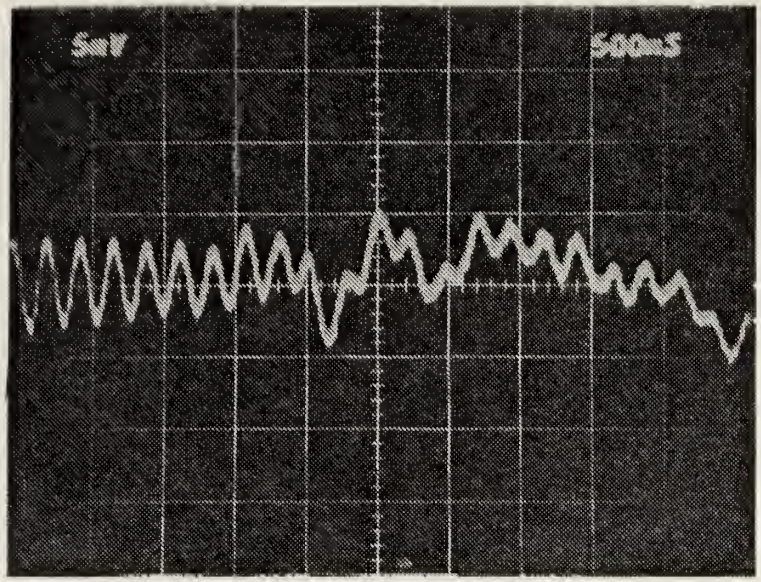

Figure 22

Typical Pulse for 2000/3000 System
at Atmospheric Pressure

Horizontal Scale: 500 nsec/cm

Vertical Scale: 5 mV/cm

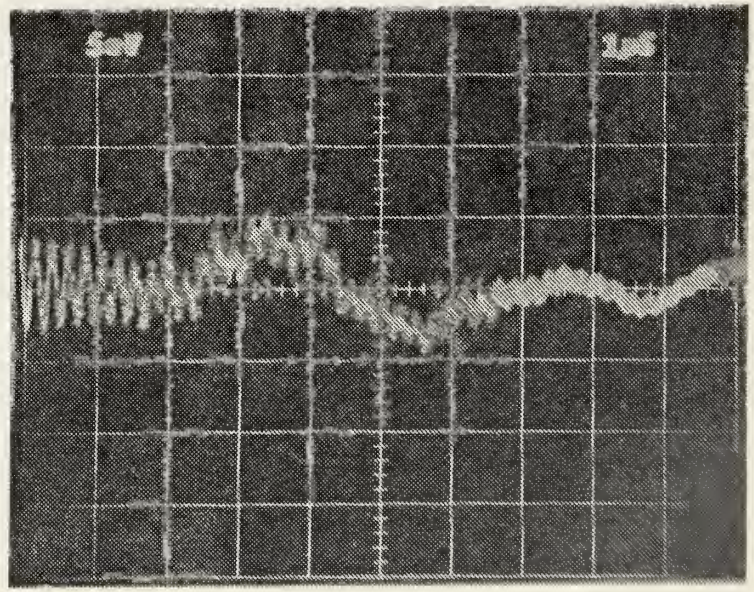

Figure 23

Typical Pulse for 0/5000 System
at Atmospheric Pressure

Horizontal Scale: 1 μsec/cm

Vertical Scale: 5 mV/cm

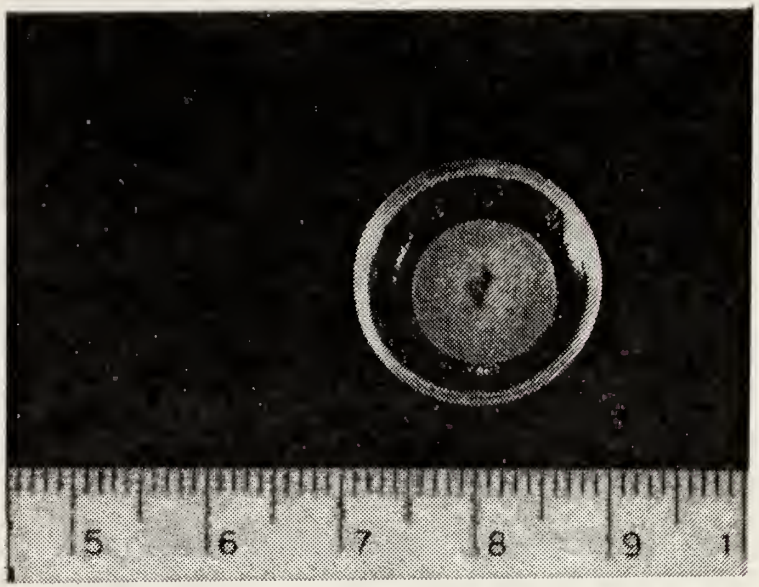

Figure 24

Surface of 2000/3000 System
after Fourteen Shots

A: Back End of CO_2 Laser Resonant Cavity (f = 3.0 m. Copper Mirror)
B: Germanium Mirror (Front End of Laser Resonant Cavity)
C: He-Ne Laser (For Rough Alignment Only)
D: f = 1.0 m. Copper Mirror
E: Ballistic Thermopile
F: Millimicro Voltmeter
G: Lucite Box Containing CO_2 Laser Cathode-Anode Assembly

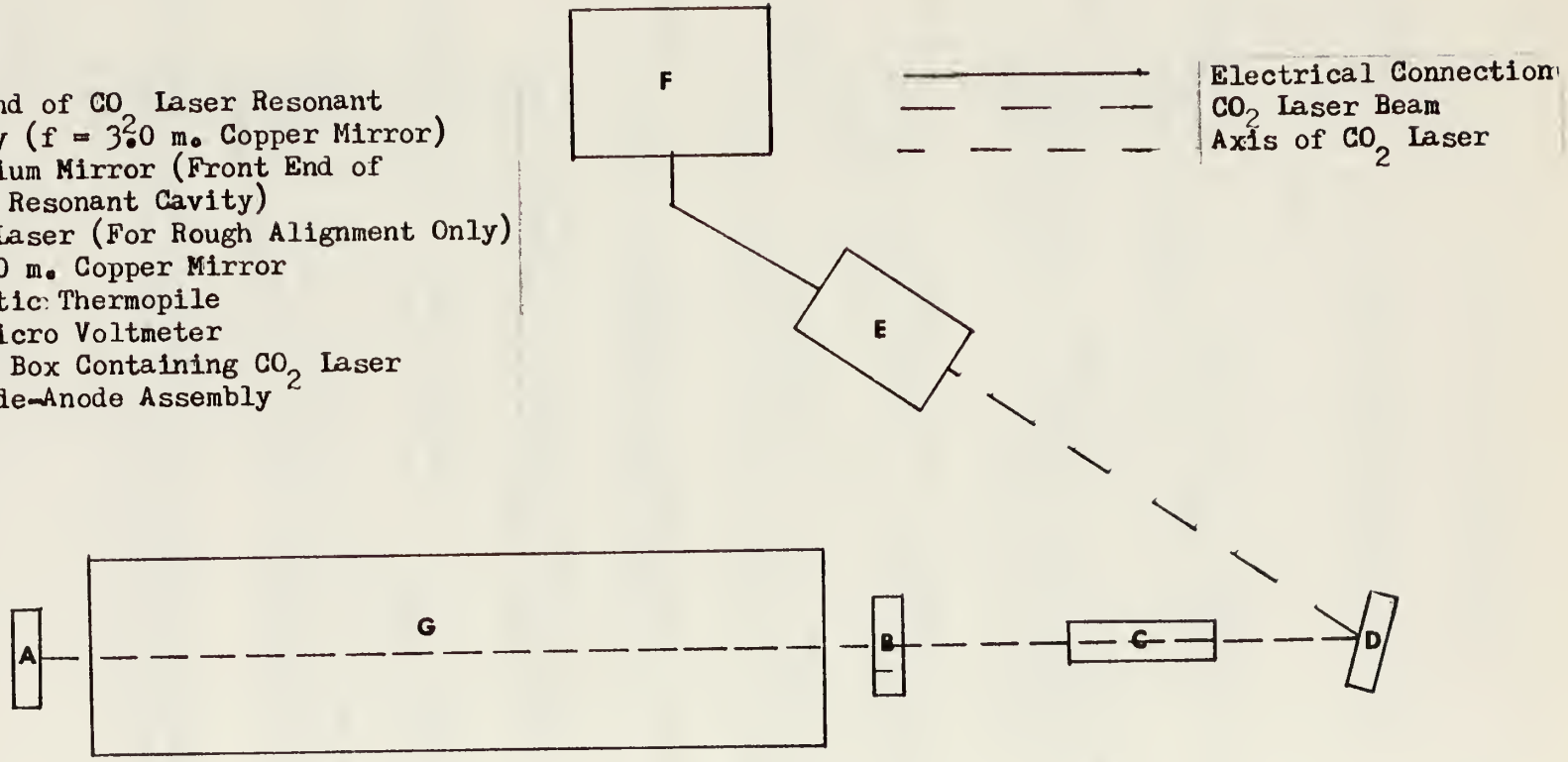

Diagram of CO_2 Laser Alignment Procedure

Figure 25

LIST OF REFERENCES

1. Angris, S. W., Direct Energy Conversion, 2nd ed., p. 228, Allyn and Bacon, Inc., 1971.

2. Ibid, p. 200-228.

3. Giuliani, J. F., "Electrical Effects in Laser-Damaged Phototransistors," J. Appl. Phys., v. 45, p. 4993-4996, November 1974.

4. Marquardt, C. L., Giuliani, J. F., and Fraser, F. W., "Observation of Impurity Migration in Laser-Damaged Junction Devices," Radiation Effects, v. 23, p. 135-139, 1974.

5. Graham, R. A., and others, "Piezoelectric Current from Shock-loaded Quartz, a Submicrosecond Stress Gauge," J. Appl. Phys., v. 36, p. 1775-1783, May 1965.

6. Jones, G. A., and Halpin, W. J., "Shorted Guard-Ring Quartz Gauge," Review Scientific Instruments, v. 39, p. 528-9, 1968.

7. Ready, J. F., Effects of High-Energy Laser Radiation, p. 279, Academic Press, 1971.

8. Air Force Cambridge Research Laboratories AFCRL-TR-73-0406, Laser Damage in Dielectric Coatings, by Milam, D., and others, p. 17, 10 July 1973.

9. Hopper, R. W., and Uhlmann, D. R., "Mechanism of Inclusion Damage in Laser Glass," J. Appl. Phys., v. 41, p. 4023.

10. Fersman, I. A., and Khazov, L. D., "Mechanism of Damage to a Surface during Illumination with Short Light Pulses," Soviet Journal of Quantum Electronics, v.2, January-February 1973.

11. Bass, M., "Nd:YAG Laser-Irradiation-Induced Damage to $LiNbO_3$ and KDP," IEEE Journal of Quantum Elect., v. QE-7, p. 350-359, July 1971.

12. Ready, J. F., p. 288-290.

13. Hughes Research Laboratories Project 2042 Semiannual Technical Report Number 2, Laser-Induced Damage in Optical Materials by C. R. Giuliano, p. 3, July 1973.

14. Wang, V., and others, "Pulsed CO_2 Laser Damage in Windows, Reflectors, and Coatings," Symposium on Laser Induced Damage in Optical Materials, 1974, p. 59-65.

15. Bullough, R., and Gilman, J. J., "Elastic Explosions in Solids Caused by Radiation," J. Appl. Phys., v. 37, p. 2283-2287, May 1966.

16. Ready, J. F., p. 364.

17. Askar'yan, G. A., and Moroz, E. M., "Pressure on Evaporation of Matter in a Radiation Beam," Sov. Phys. JETP, v. 16, p. 1683, December 1962.

18. Skeen, G. H., and York, C. M., "Laser-Induced 'Blow-off' Phenomena," Appl. Phys. Lett., v. 12, p. 369-371, 1 June 1968.

19. Krehl, P., Schwirzke, F., and Cooper, A. W.,"Correlation of Stress-Wave Profile and the Dynamics of the Plasma Produced by Laser Irradiation of Plane Solid Targets," J. Appl. Phys., v. 46, p. 4400-4406, October 1975.

20. Pirri, A. N., "Theory for Momentum Transfer with a High-Power Laser," Phys. Fluids, v. 16, p. 1435-1440, September 1973.

21. Dyer, P. E., and others, "Interaction of High-Power CO_2 Lasers with Solid Targets," in Laser Interaction and Related Plasma Phenomena, Vol. 3A, edited by H. J. Schwarz and H. Horn, p. 191, Plenum Press, 1973.

22. Pirri, A. N., Schier, R., and Northam, D., "Momentum Transfer and Plasma Formation above a Surface with a High-Power CO_2 Laser," Appl. Phys. Lett., v. 21, p. 79-81, 1 August 1972.

23. Naval Postgraduate School Technical Report NPS-61-61Nb 75121, Laser Effects Handbook, Chapter 3, by Harrison, D. E., Jr., p. 3, December 1975.

24. Gregg, D. W., and Thomas, S. J., "Momentum Transfer Produced by Giant Laser Pulses," J. Appl. Phys., v. 31, p. 2787-2789, June 1966.

25. Anderholm, N. C., "Laser-Generated Stress Waves," Appl. Phys. Lett., v. 16, p. 113-115, 1 February 1970.

26. McMordie, J. A., and Roberts, P. D., "The Interaction of Pulsed CO_2 Laser Radiation with Aluminum," J. Phys. D: Appl. Phys., v. 8, p. 768-781, 11 May 1975.

27. Fox, J. A., "Effect of Water and Paint Coatings on Laser-Irradiated Targets," Appl. Phys. Lett., v. 10, p. 461-464, 15 May 1975.

28. Yang, L. C., "Stress Waves Generated in Thin Metallic Films by a Q-switched Laser," J. Appl. Phys., v. 45, p. 2601-2607, June 1974.

29. Magee, T. J., Armistead, R. A., and Krehl, D., "Laser-Induced Stress in Coated and Uncoated Targets," J. Phys. D. Appl. Phys., v. 8, p. 498-504, 1975.

30. Strickland, H. W., Modifications to and Investigations of Arc Formation in a CO_2 TEA Laser, Masters Thesis, Naval Postgraduate School, Monterey, California, 1974.

31. Behrens, P., Breakdown Phenomena in Rare and in Molecular Gases Using Pulsed Carbon Dioxide Laser Radiation, Masters Thesis, Naval Postgraduate School, Monterey, California, 1974.

32. Stevenson, P. W., Spectroscopic Examination of Carbon Dioxide Laser Produced Gas Breakdown, Masters Thesis, Naval Postgraduate School, Monterey, California, 1975.

33. Radio Corporation of America Laboratories, Princeton, New Jersey, Contract Number AF33(615)-2259, Improved Thin Film Solar Cells, by Perkins, D. M., and others, p. 14-25.

34. Carslaw, H. S., and Jaeger, J. C., Conduction of Heat in Solids, 2nd ed., p. 256, Oxford University Press, 1959.

35. American Institute of Physics Handbook, 3rd ed., McGraw-Hill, 1972.

36. Heavens, O. S., Optical Properties of Thin Films, pp. 76-77, Academic Press, Inc., 1955.

37. Air Force Cambridge Research Laboratories Technical Report 72-0170, Compendium on High Power Infrared Laser Materials, by Sahagian, C. S. and Pitha, C. A., March 1975.

38. Davis, L. J., Self-Generated Magnetic Fields Produced by Laser Bombardment of a Solid Target, Masters Thesis, Naval Postgraduate School, Monterey, California, 1972.

39. Michaels, J. E., "Thermally Induced Elastic Wave Propagation in Slender Bars," in Proceedings of the Third U. S. National Congress of Applied Mechanics, 1958, p. 209-213, The American Society of Mechanical Engineers, 1958.

40. Griffith, M. V., and Horton, G. K., "The Transient Flow of Heat through a Two-Layer Wall," Phys. Soc. LVIII, 4, p. 481-487.

41. Ready, J. F., p. 161.

42. Ibid, p. 117.

43. Lawrence Livermore Laboratory Report Number UCRL-51488, A Theoretical Description of the Interaction of a Pulsed Laser and a Target in an Air Environment, by Edwards, A., and others, p. 67-69, 20 November 1973.

INITIAL DISTRIBUTION LIST

		No. Copies
1.	Defense Documentation Center Cameron Station Alexandria, Virginia 22314	2
2.	Library, Code 0212 Naval Postgraduate School Monterey, California 93940	2
3.	Department Chairman, Code 61 Department of Physics and Chemistry Naval Postraduate School Monterey, California 93940	2
4.	Professor A. W. Cooper, Code 61 Cr Department of Physics and Chemistry Naval Postgraduate School Monterey, California 93940	4
5.	Assoc. Professor F. Schwirzke, Code 61 Sw Department of Physics and Chemistry Naval Postgraduate School Monterey, California 93940	1
6.	Dr. T. J. Magee Stanford Research Institute 333 Ravenswood Avenue Menlo Park, California 94205	1
7.	LT John Frank Jacobson, USN 1931 South 28 Street Omaha, Nebraska 68105	2

Thesis 166522
J2375 Jacobson
c.1 Examination of laser-produced pressure pulses in a gallium arsenide solar cell.